AD 400 680



63-3-1



RADC-TDR-62-446

# THE DESIGN AND CONSTRUCTION OF A HIGH-POWER UHF CRESTATRON

TECHNICAL DOCUMENTARY REPORT NO. RADC-TDR-62-446

August, 1962

Techniques Laboratory
Rome Air Development Center
Research and Technology Division
Air Force Systems Command
United States Air Force
Griffiss Air Force Base New York



Project No. 5573, Task No. 557303

(Prepared under Contract No. AF 30(602)-2834
by Electron Physics Laboratory, Department of Electrical Engineering
The University of Michigan, Ann Arbor, Michigan
Author: G. T. Konrad)

## FOREWORD

This report was prepared by the Electron Physics Laboratory, Department of Electrical Engineering, The University of Michigan, Ann Arbor, Michigan, on Air Force Contract No. AF 30(602)-2834 under Project No. 5573 of Task No. 557303 entitled "The Design and Construction of a High-Power UHF Crestatron". The secondary report number is Technical Report No. 52 under Project 05228.

The author gratefully acknowledges the work done by Mr. J. W. Ward on this program. He also is grateful to Messrs. H. K. Detweiler and J. Loh for carrying out some of the experimental work.

The work was administered under the direction of the Techniques Laboratory, Rome Air Development Center. Lt. J. Schneider was the project engineer.

AIR FORCE, Cato Show Prtg. Co. 3/28/63 - 280

ABSTRACT

The design, construction and experimental tests of a pulsed, high-power uhf Crestatron are described. The design procedures outlined in this report are useful for the construction of Crestatrons in general. The data presented shows the operating characteristics of the Crestatron under small-signal as well as large-signal conditions. In addition some experiments on the harmonic output of the Crestatron are described.

**PUBLICATION REVIEW**

**This report has been reviewed and is approved.**

**Approved:** Paul M. Baldum for Lt Col USAF

**ARTHUR J. FROHLICH**
**Chief, Techniques Laboratory**
**Directorate of Aerospace Surveillance & Control**

**Approved:** Paul M. Baldum for Lt Col USAF

**WILLIAM T. POPE**
**Acting Director**
**Director of Aerospace**
**Surveillance & Control**

TABLE OF CONTENTS

## LIST OF ILLUSTRATIONS

LIST OF TABLES

# THE DESIGN AND CONSTRUCTION OF A HIGH-POWER UHF CRESTATRON

## INTRODUCTION

The Crestatron invented some time ago by Rowe[1] is a forward-wave amplifier which like the backward-wave oscillator operates on a beating-wave principle. However, there is an important difference between the operation of these two devices. Since the Crestatron uses a forward wave the density modulation in the stream and the circuit field producing this modulation travel in the same direction resulting in an inherently more efficient type of operation. Typical efficiencies are 20-25 percent compared to 3-5 percent for BWO's and BWA's. The Crestatron is a device having moderate gain (10-15 db), high efficiency and short length. In some applications the magnet can be eliminated because of the short length of the r-f structure.

This report describes the design and construction of a high power uhf Crestatron designed to have a power output of 5-10 kw (pulsed) in the 300-900 mc frequency range with at least 10 db gain and a minimum saturation efficiency of 25 percent. Experimental results are presented for the five tubes which have been built. These tubes are similar except for minor differences in the construction of the electron gun which provides a confined flow hollow beam and the length of the r-f interaction structure. The circuit used in these tubes is a single-filar helix supported in a glass envelope by sapphire rods. Coupled helices are used for the input and output transducers.

## PRINCIPLES OF CRESTATRON OPERATION

As mentioned above, the Crestatron operates in the beating-wave rather than the growing-wave regime. The two beating waves in the Crestatron are the slow space-charge wave and the circuit wave, the fast wave being negligibly excited. These waves are excited with purely real amplitudes when the voltage is high enough so that Pierce's growing-wave parameter $x_1$ is zero. At the input the voltage on the r-f structure is due to the slow space-charge wave $V_{c1}$ and the circuit wave $V_{c2}$. These are exactly 180 degrees out of phase and combine to produce the applied voltage. Farther down stream they add in phase because their propagation constants are slightly different, typically at a length where $CN_s \approx 0.50$.

Crestatron gain is primarily a function of $\Delta b$, where

$$\Delta b \triangleq b - b_{x_1=0} \tag{1}$$

and

$$b = \frac{1}{C}\left(\frac{u_o}{v_p} - 1\right) . \tag{2}$$

As $\Delta b$ approaches zero the two waves have nearly the same propagation constant. Therefore a compromise must be made between length and gain since the maximum gain increases as $\Delta b$ approaches zero, while the length to achieve this high gain increases. Typical values of $\Delta b$ for 10 db gain at $CN_s = 0.50$ are around 0.20. As in the traveling-wave amplifier it is desirable to have a high value of the gain parameter, C, and a low value of the space-charge parameter, QC, for high efficiency operation. The gain of the Crestatron can be calculated using the small-signal theory of the traveling-wave tube. Thus the gain in db is given by

$$G = 10 \log \left| \left( \frac{V_z}{V} \right)^2 \right| , \qquad (3)$$

where

$$\frac{V_z}{V} = e^{\frac{-j\theta}{C}} \sum_{i=1}^{3} \left( \frac{V_i}{V} \right) \left( \frac{V_{ci}}{V_i} \right) e^{\delta_i \theta} ,$$

$$\theta = \beta_e C z = 2\pi C N_s ,$$

$$\delta_i = x_i + j y_i . \qquad (4)$$

The incremental propagation constants $\delta_i$ can be obtained from the familiar quartic determinantal equation which is a function of C, QC, and the loss parameter d. Gain vs. distance is plotted in Fig. 1 for C = 0.25, QC = 0.25 and b = 3.4 for different values of the loss parameter d. It is seen that the gain for short tubes is reduced as loss is increased. However, for tubes longer than $CN_s \approx 1.5$, the loss has actually increased the gain over the no loss case. The reason for this is that while the circuit wave is attenuated at a rate approximately proportional to d, the slow space-charge wave must grow in amplitude because of its negative energy; i.e., the beam has less energy in the presence of the slow space-charge wave than in its absence. At these long lengths the "growing" slow space-charge wave predominates and produces more gain than purely beating-wave gain. The fact that $x_1$ never goes to zero when loss is present is another way of seeing that $V_{c1}$ grows with distance, although it should be remembered that this finite $x_1$ arises not from close coupling between the circuit wave and the slow space-charge wave as in the growing-wave region but simply because loss is present. This type of interaction at sufficiently high values of d between purely beating-wave gain and

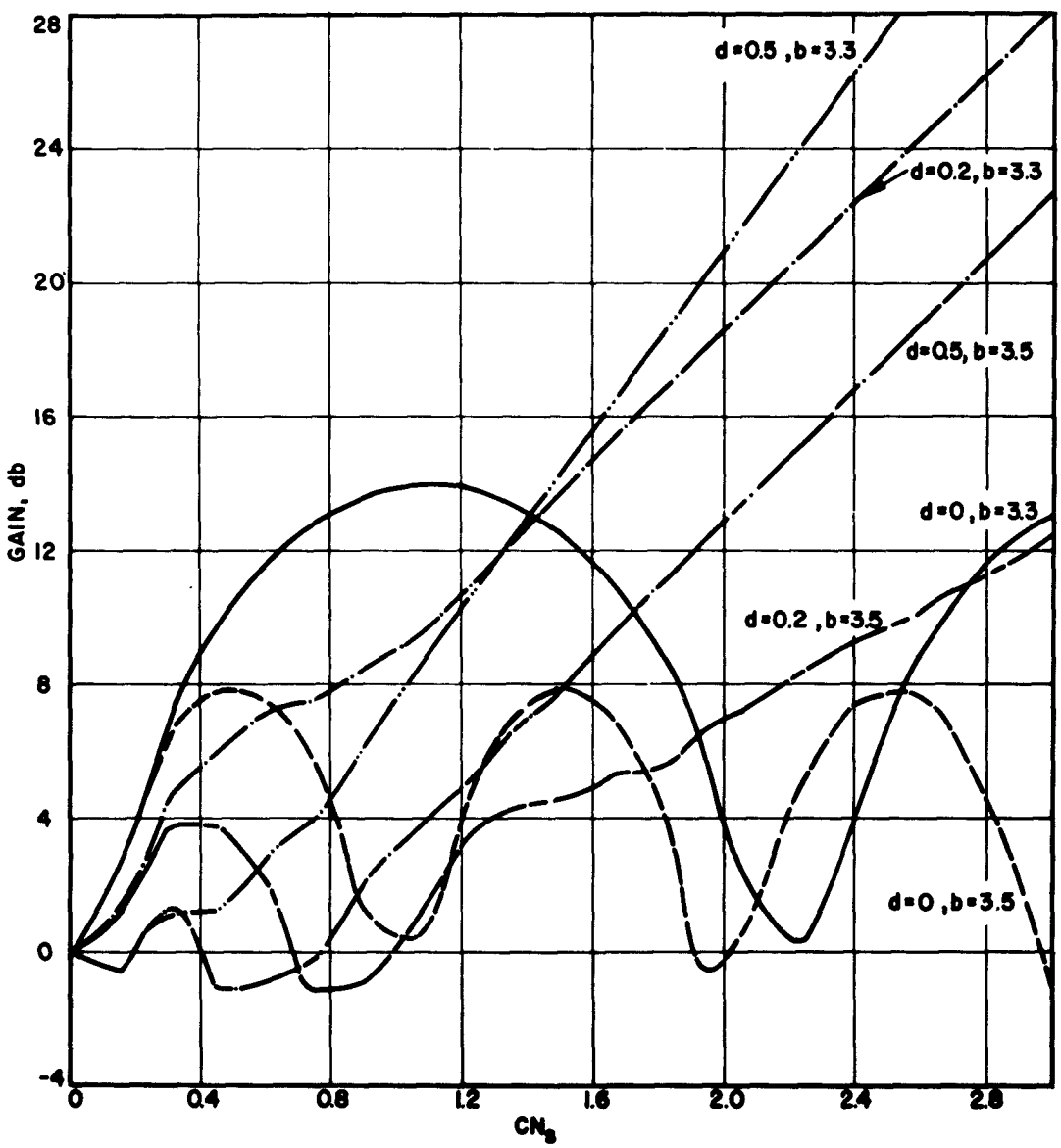


FIG. 1 GAIN VS. DISTANCE. (C = 0.25, QC = 0.25,

$b_{x_1} \cong 3.26$, $b \cong 3.4$)

growing-wave gain might best be described as a beating-wave resistive-wall amplification.

## GENERAL DESIGN CONSIDERATIONS

A brief summary of the approach taken in designing helix-type Crestatrons follows. The main problem is to keep the relative injection velocity, b, constant over the frequency range of operation. The quantity $\Delta b$, which determines the maximum Crestatron gain, is then nearly constant because $b_{x_1=0}$ is a slowly varying function of C and QC. To keep b constant requires both low dispersion and low impedance variation across the frequency band. For wide bandwidths these two requirements usually necessitate having a helix with a metal shield surrounding it, ordinarily with a shield-to-helix radii ratio between 1.4 and 2.0.

The first step in the design procedure is to choose a beam power from the desired r-f power output and the expected efficiency. For most Crestatrons with hollow beams, 25 percent is a conservative efficiency to use in this step. Next, a low-frequency value of ka is chosen which, together with the frequency range, should determine an inside circuit diameter consistent with current density limitations. From the beam voltage and the fact that $1+Cb \approx 1.5$ for most Crestatrons with hollow beams, the low-frequency $\gamma a$ can be calculated using

$$\frac{u_o}{v_p} = 1 + Cb = \frac{\sqrt{V_o}}{506} \frac{\gamma a}{ka} . \qquad (5)$$

If this value of $\gamma a$ is in the range 0.5 to 1.0, the approximate $v_p/c$ required can be calculated and a shield-to-helix radii ratio can be selected in the range of 1.4 - 2.0. At this point it is necessary to

estimate the probable DLF, preferably from a tube already constructed in this frequency range, which uses similar geometry and materials in supporting the r-f circuit. A trial helix design can be made by using

$$\frac{v_p}{c} \simeq \frac{1}{(\cot\psi)_{sheath}} = \frac{DLF}{(\cot\psi)_{actual}} \qquad (6)$$

or

$$p \simeq \frac{2\pi a}{DLF}\left(\frac{ka}{\gamma a}\right) . \qquad (7)$$

Now $v_p/c$ and $1 + Cb$ vs. frequency can be calculated for this helix design. From a chosen beam geometry b and C may now be calculated; b should be around 2.5 to 3.0, depending on the value of QC found from

$$QC = \frac{1}{4C^2}\left(\frac{\frac{\omega_q}{\omega}}{1 + \frac{\omega_q}{\omega}}\right)^2 , \qquad (8)$$

where

$$\frac{\omega_q}{\omega} = \left(\frac{\omega_q}{\omega_p}\right)\left(\frac{\omega_p}{\omega}\right) = R\frac{\omega_p}{\omega}$$

and

$$\omega_p = 1.83 \cdot 10^8 \sqrt{\frac{J_o}{V_o^{1/2}}} , \qquad (9)$$

where $J_o$ = d-c current density and

$V_o$ = d-c beam voltage.

The plasma frequency reduction factor, R, can be found from Branch and Mihran[2], who have presented graphs of R vs. $\gamma a$ for different beam geometries.

As mentioned previously, Crestatron gain and efficiency depend primarily upon having the proper injection velocity which results in $\Delta b$ being slightly positive. Figure 2 shows b as a function of C for different values of $u_o/v_p$ and also $b_{x_1=0}$ as a function of C with QC as the parameter. This graph greatly facilitates finding $\Delta b$ for a given $u_o/v_p$, C and QC. If $\Delta b$ is not in the range of 0.10 to 0.30 in a first design, either the voltage or helix pitch must be adjusted to bring $\Delta b$ into the aforementioned range. Once $\Delta b$, C and QC as a function of frequency are known, maximum Crestatron gain can be found using Reference 1. A length can be calculated by making $CN_s \approx 0.35$ at the low-frequency end. Efficiency and gain vs. frequency can then be calculated for different drive levels.

## HELIX DESIGN AND COLD TEST MEASUREMENTS

The circuit used in this tube is a single-filar molybdenum helix supported in a precision-bore Nonex envelope by three sapphire rods. In the first three tubes constructed the rods were notched at each helix turn in order to insure good alignment. It was found, however, that the rods and helix envelope had a tendency to break during processing of the tube. Consequently in the last two tubes rods with ground flats were used. The helix was found to be sufficiently rigid to hold its shape with this arrangement. Some difficulty was experienced with early helices which were wound on a stainless steel mandrel. When the helix was fired the difference in expansion between the molybdenum and stainless steel caused a permanent spring-out, making it difficult to load the helix into the glass envelope without breaking the sapphire rods which were required

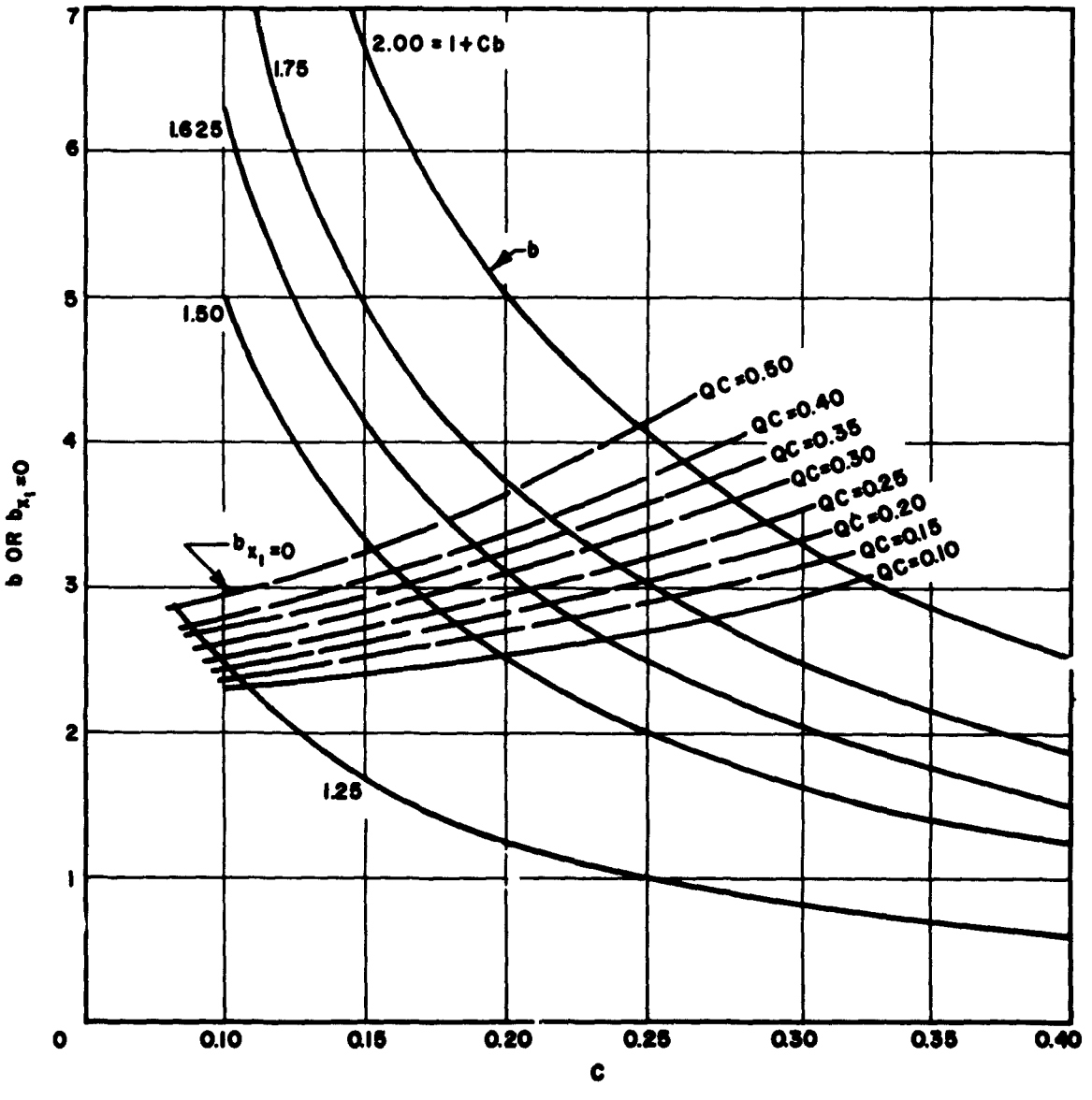


FIG. 2 $b_{x_1=0}$ VS. C WITH QC AS A PARAMETER AND b VS. C WITH 1 + Cb AS A PARAMETER.

to hold the helix in compression. This problem was eliminated by utilizing a molybdenum mandrel.

The electrical design of the helix follows the method outlined above. Table I summarizes the final design parameters of the helix.

Table I

Uhf Helix Parameters

| | |
|---|---|
| Pitch: | 0.250 inch |
| cot $\psi$: | 9.45 |
| Mean Diameter: | 0.752 inch |
| Wire Diameter: | 0.100 inch |
| Material: | Molybdenum |
| Helix Supports: | 0.080-inch sapphire rods |
| ka at 300 mc: | 0.06 |

The measured phase velocity and DLF for this helix design are shown in Fig. 3 for an unshielded helix and for a shield-to-helix radii ratio of 1.5. It is seen that the shield greatly reduces the dispersion from the unshielded case. Of course the penalty is essentially an increase in tube length because C is lowered approximately 25 percent at 300 mc and approximately 10 percent at 900 mc. A gradual increase in phase velocity from 300 to 900 mc may be noted for the shielded helix. This negative dispersion behavior[3] results from the dielectric surroundings producing an effective shunt capacity per unit length which decreases with increasing frequency. At low frequencies the electric field extends farther into the dielectric and effectively increases the energy storage and reduces the helix impedance.

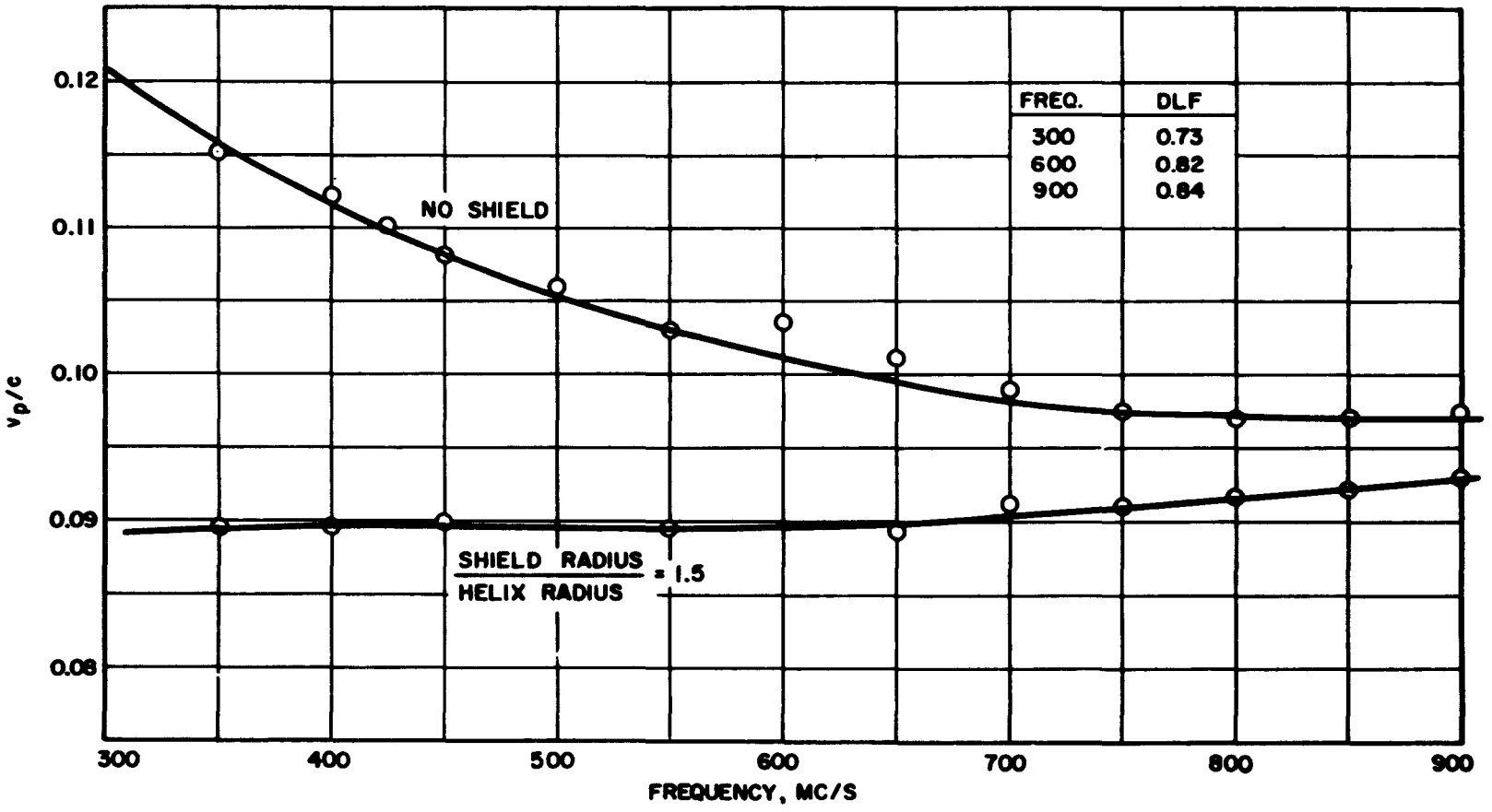


FIG. 3 MEASURED PHASE VELOCITY VS. FREQUENCY.

An interesting fact useful in comparing the shielded and unshielded sheath helix is shown in Fig. 4, where the ratio of the phase-to-group velocities, $v_p/v_g$, is plotted versus $\gamma a$. It is seen that for an unshielded helix a $\gamma a$ lower than approximately 0.80 results in a rapid increase in dispersion because of the rapid rise in $v_p/v_g$ at this point. The reverse may be noted for the shielded helix. Of course this property could not be used for high-power tubes at higher frequencies than perhaps S-band because the inside diameter of the structure and beam-power considerations would not allow the low $\gamma a$ permitted by dispersion considerations. However, for most uhf and vhf tubes, current density limitations are not present and for many cases the increased bandwidth resulting from negligible dispersion will compensate for the reduction in C and the increase in length, especially for low-gain tubes such as Crestatrons.

It is recalled that the phase velocity $v_p$ and the group velocity $v_g$ are given by

$$v_p = \frac{ka}{\gamma a} = \frac{\omega}{\beta} \tag{10}$$

and

$$v_g = \frac{\partial \omega}{\partial \beta} \ . \tag{11}$$

Ayers[4] has arrived at the frequency bandwidth corresponding to a change in b (or $\Delta b$), which is as follows:

$$\frac{\Delta \omega}{\omega} = \frac{v_p}{u_o} \frac{C \Delta b}{\left( \frac{v_p}{v_g} - 1 \right)} \quad \text{(for constant C)} \ . \tag{12}$$

For the Crestatron[5] the exact change in gain due to a change in b is a complicated function of C, QC, b and $CN_s$. However, a good approximation to the maximum bandwidth can be made using Eq. 12. For most

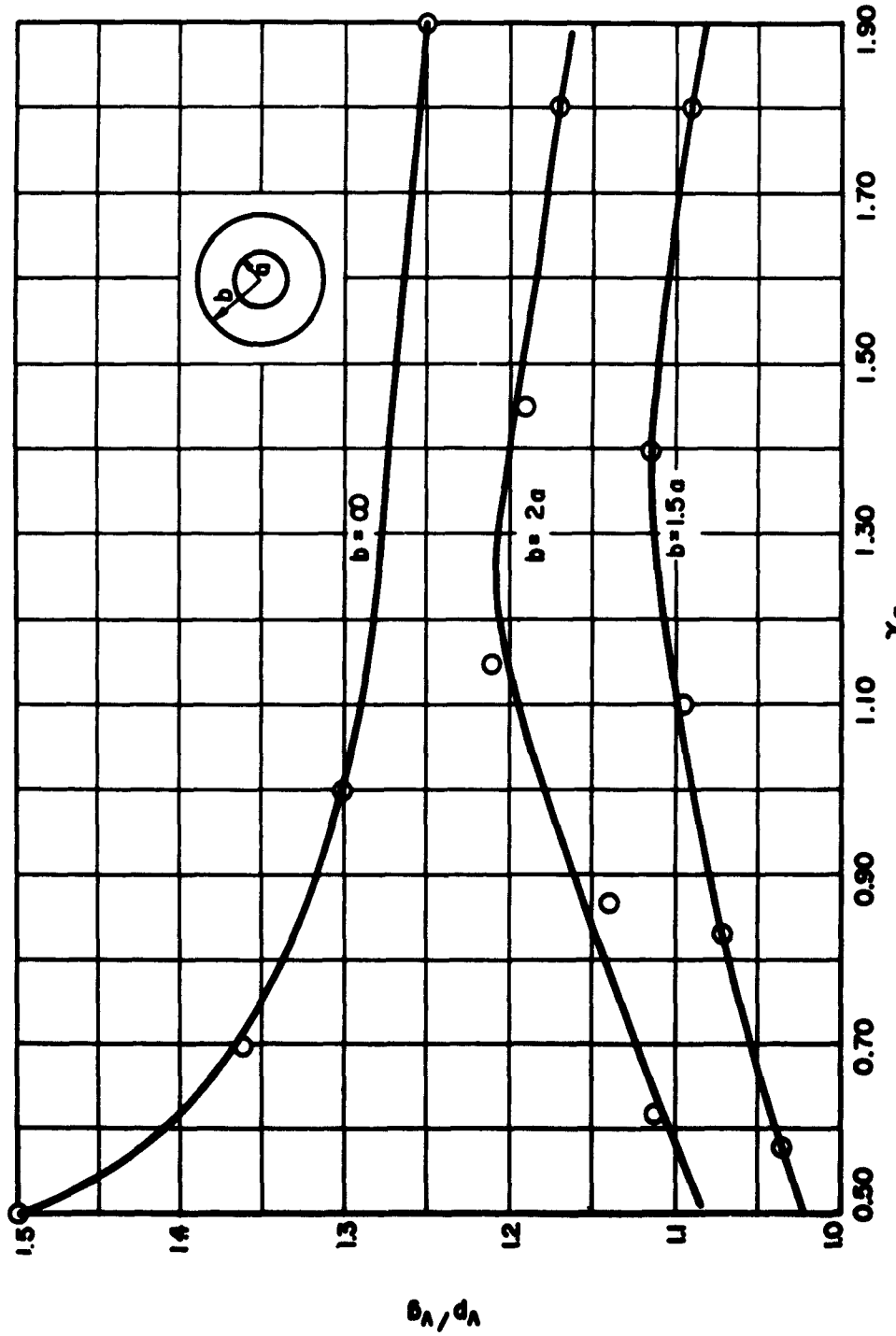


FIG. 4 CALCULATED RATIO OF PHASE TO GROUP VELOCITY FOR SHEATH HELIX WITH EXTERNAL SHIELD.

Crestatron designs the gain has dropped about 3 db for $\Delta b \cong 0.60$. Usually $u_o/v_p \cong 1.5$ for high-C tubes. From Fig. 4 $v_p/v_g \approx 1.10$ for a shield-to-helix radii ratio of 1.5. Thus, for C = 0.25

$$\frac{\Delta\omega}{\omega} = \frac{1}{1.5} \frac{(0.25)(0.60)}{[1.10-1.0]} \approx 1$$

or a 3 to 1 bandwidth. This wide bandwidth is also evident from the gain vs. distance curves.

## HELIX-IMPEDANCE MEASUREMENTS

Experimental measurements using a method described by Lagerstrom[6], where a dielectric rod perturbs mainly the TE fields at the axis of the helix, were used to measure the helix impedance. A 0.100-inch diameter sapphire rod was inserted on the axis and the resulting change in phase was noted by observing the shift in the position of the minimum on a slotted line in one arm of a phase bridge. The change in the position of a minimum, $\Delta x$, when using a dielectric rod of radius b with dielectric constant $\epsilon'$ is related to the impedance on the axis K (r=0) as follows:

$$K\,(r = 0) = \frac{480\left(\frac{\Delta x}{D}\right)}{(\gamma b)^2(\epsilon'-1)p_e}\ (\text{ohms}) \quad , \tag{13}$$

where D is the physical length of the slow-wave structure tested and $p_e$ is a shape factor to account for the finite size of the perturbing rod. For a hollow-beam tube this impedance may be transformed at $r = r_o$, using

$$K\,(r = r_o) = K\,(r = 0)\ I_o^2(\gamma r_o) \quad . \tag{14}$$

The above assumes the beam is thin enough so that the field does not vary across it. This is nearly true for the hollow beam used in this tube,

which has a thickness of 0.030 inch compared to a mean diameter of 0.507 inch. It was quite difficult to obtain reproducible results because the VSWR of the couplers used was not sufficiently low for the phase bridge setup employed in these measurements. Because of this, no experimental impedance measurements were made for the shielded helix case for which the VSWR was relatively high. Instead the interaction impedance for the shielded helix was computed from the experimental data for the unshielded helix and Reference 7. Figure 5 shows the impedance for the two cases. Fairly good agreement between the theoretical and measured values was obtained for the unshielded helix.

## HOLLOW-BEAM GUN

A schematic drawing of the hollow-beam guns used in the first two tubes is shown in Fig. 6. The center anode electrode in these tubes was held by a spoke spot-welded to the inside of the outer anode below the cathode assembly. Because of assembly difficulties with this method, in Tube No. 3 the center electrode was held by three 0.005-inch molybdenum tabs going directly to the outer anode. Figure 7 shows a picture of the latter gun, which is identical to the previous guns except for the different support method for the center anode.

This gun is a conventional, immersed, rectilinear-flow Pierce gun which was designed to operate with the focus electrodes at cathode potential. The cathode-anode distance was chosen to give a microperveance per square of 0.13 and a total microperveance of 5.9. The cathode was a Phillips Type B in the first four tubes and a Semicon Type S cathode in Tube No. 5. The emitting surface is 0.025-inch wide and has a mean

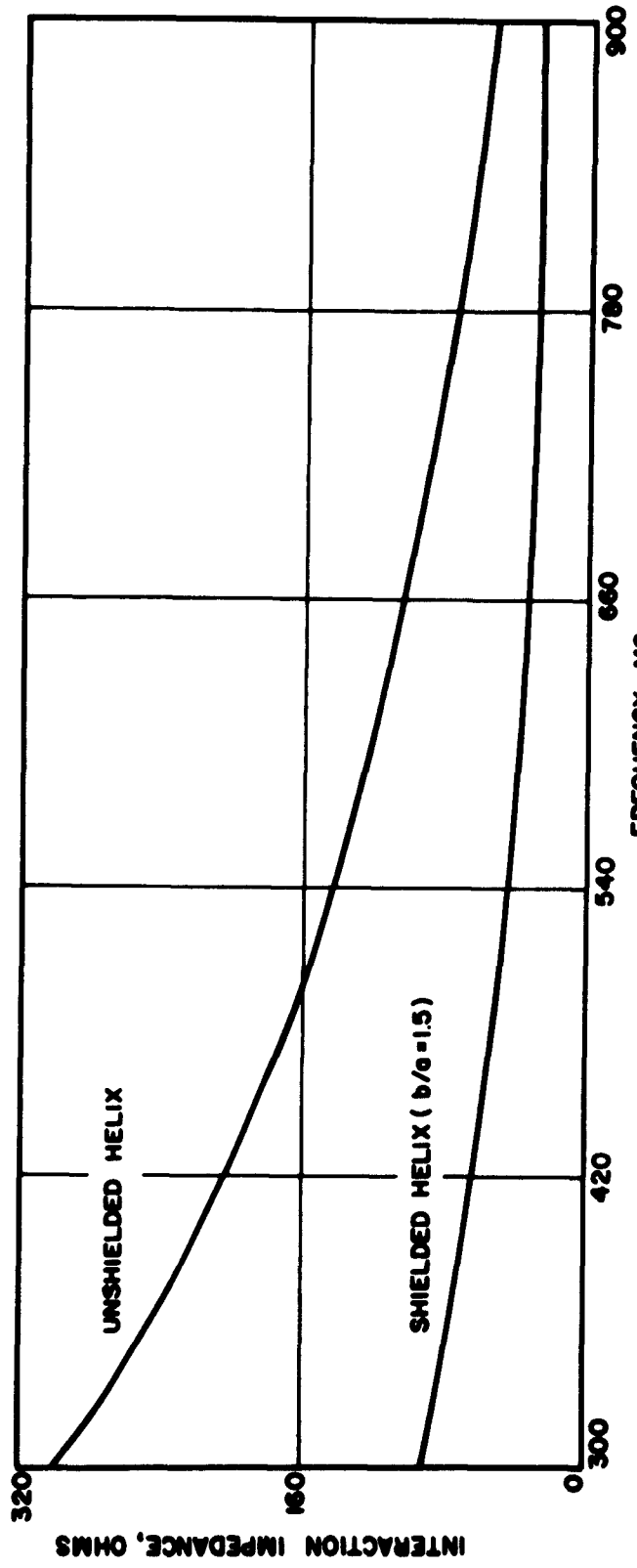


FIG. 5 INTERACTION IMPEDANCE FOR THE UHF CRESTATRON.

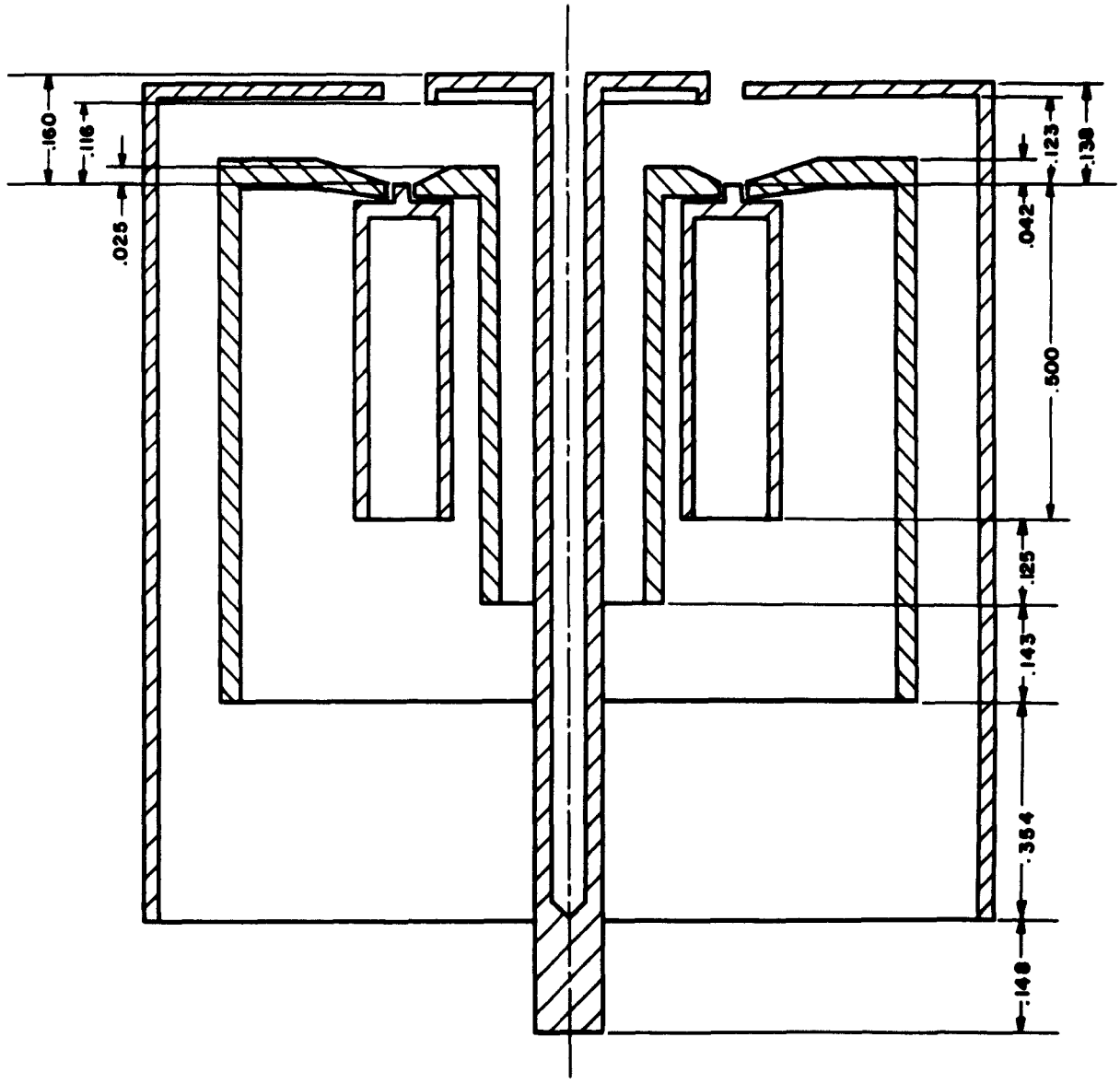


FIG. 6 SCHEMATIC DRAWING OF A HOLLOW-BEAM ELECTRON GUN.

FIG. 7 UHF HOLLOW-BEAM GUN.

diameter of 0.507 inch. The electrodes are molybdenum cylinders held by supports attached to a Vicor disk which can be seen in Fig. 7.

The diode characteristics of the gun used in Tube No. 1 are shown in Fig. 8. A current of 3 amperes corresponds to a current density of $\approx$ 10 amps/cm$^2$. The perveance drops from 6.5 microperes to 4 microperes as the voltage is raised from 6 to 10 kv. No evidence of voltage breakdown has been noted at voltages up to 10 kv.

## AMPLIFIER DESIGN

The electrical parameters resulting from the design procedure outlined above using the helix and beam described previously are shown in Tables II and III.

Table II

Summary of Electrical Design Parameters

| | |
|---|---|
| Design Beam Voltage | = 6 kv |
| Design Beam Current | = 3.1 amp |
| Current Density | = 10 amps/cm$^2$ |
| Perveance | = 5.9 micropervs |
| $u_o/c$ | = 0.153 |
| Mean Helix Radius | = 0.376 inch |
| Mean Beam Radius | = 0.254 inch |

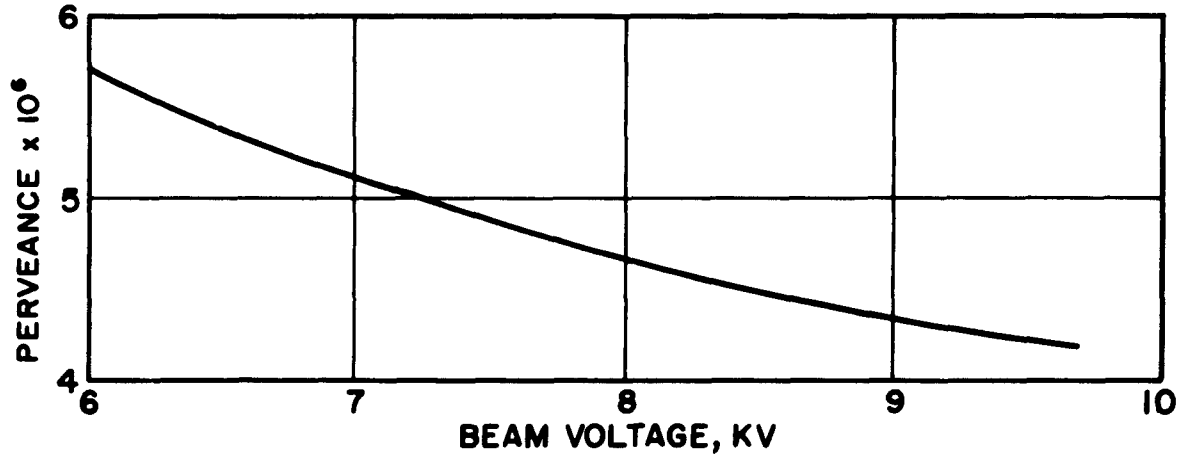


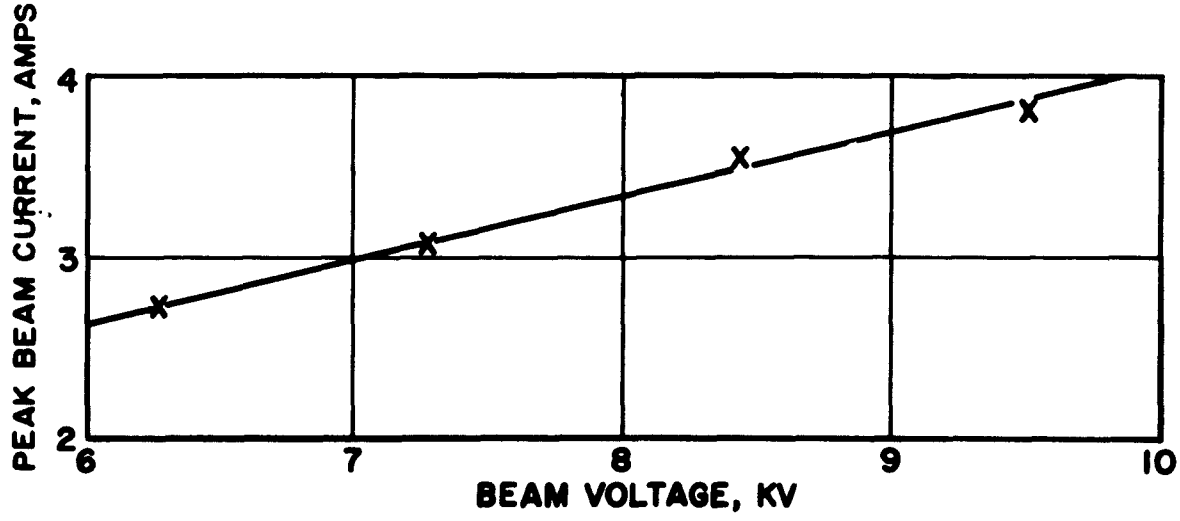


FIG. 8 PERVEANCE AND BEAM CURRENT VS. BEAM VOLTAGE FOR UHF CRESTATRON HOLLOW-BEAM GUN.

Table III

Operating Parameters of the Uhf Crestatron

| Freq. (mc.) | 300 | 400 | 500 | 600 | 700 | 800 | 900 |
|---|---|---|---|---|---|---|---|
| ka | 0.06 | 0.08 | 0.10 | 0.12 | 0.14 | 0.16 | 0.18 |
| DLF | 0.73 | 0.76 | 0.79 | 0.82 | 0.82 | 0.82 | 0.84 |
| $v_p/c$ | 0.089 | 0.089 | 0.090 | 0.090 | 0.091 | 0.092 | 0.093 |
| $\gamma a$ | 0.675 | 0.895 | 1.11 | 1.34 | 1.55 | 1.75 | 1.94 |
| $kr_o$ | 0.041 | 0.054 | 0.067 | 0.081 | 0.094 | 0.108 | 0.121 |
| $\gamma r_o$ | 0.455 | 0.603 | 0.749 | 0.900 | 1.05 | 1.18 | 1.31 |
| Impedance Reduction Factor: $F=F_1F_2$ | 0.43 | 0.44 | 0.49 | 0.53 | 0.52 | 0.51 | 0.51 |
| K(ohms) | 260 | 182 | 147 | 112 | 81.1 | 60.8 | 46.5 |
| R | 0.115 | 0.14 | 0.16 | 0.18 | 0.195 | 0.21 | 0.225 |
| $\omega_q/\omega$ | 0.430 | 0.392 | 0.358 | 0.337 | 0.320 | 0.294 | 0.285 |
| C | 0.239 | 0.228 | 0.218 | 0.214 | 0.191 | 0.183 | 0.179 |
| QC | 0.39 | 0.38 | 0.36 | 0.34 | 0.40 | 0.39 | 0.38 |
| b | 3.01 | 3.12 | 3.21 | 3.27 | 3.61 | 3.66 | 3.63 |
| $b_{x_1=0}$ | 3.70 | 3.58 | 3.40 | 3.35 | 3.30 | 3.28 | 3.27 |
| $\Delta b$ | -0.69 | -0.46 | -0.19 | -0.08 | 0.31 | 0.38 | 0.36 |
| $N_s$(Interaction length = 8 inches) | 1.33 | 1.77 | 2.22 | 2.66 | 3.08 | 3.54 | 4.00 |
| $CN_s$ | 0.318 | 0.404 | 0.484 | 0.570 | 0.588 | 0.647 | 0.716 |
| Max. Gain (db) | 8.2 | 10.8 | 11.2 | 11.8 | 6.5 | 5.5 | 5.0 |

It should be pointed out that a slight change in voltage can be used to raise and optimize the gain vs. frequency curve as well as make $\Delta b$ positive everywhere, as will be shown in a later section.

## R-F TRANSITIONS

Early in the development of this project it was planned to use pin matches in which the coaxial center conductor was connected to the helix by pins passing through the glass envelope. Experiments using this method were rather disappointing. Even with a closely spaced shield surrounding the helix it appeared that the helix impedance at the low-frequency end was too high to match into a 50-ohm coaxial line. For a shield-to-helix radii ratio of 1.5 the calculated helix impedance defined on a power-current basis[7] varies from approximately 200 ohms at 300 mc to 125 ohms at 900 mc. By stretching out the last two turns a fairly good match (VSWR $\leq 2$) could be obtained from 500 to 900 mc.

Because of the marginal performance obtained with this method of coupling and due to the difficulty experienced in making a vacuum-tight and mechanically rugged seal between the pin and the glass envelope, it was decided to try a coupled-helix transition. A series of tests was made on coupled helices with different TPI's and outer shield diameters. All couplers had an I.D. = 1.13 inch, which is slightly larger than the glass envelope used. They were supported by a closely fitting glass tube which slid into the brass shield (see Fig. 9). The transition from the coaxial line to the coupling helix was made through an off-center slot cut in the end cap which permitted the center conductor of the coax to be tangential to the helix at the junction where they were soldered together. A photograph of the complete coupler carriage is shown in Fig. 10.

Best results were obtained with a coupler having the dimensions listed below:

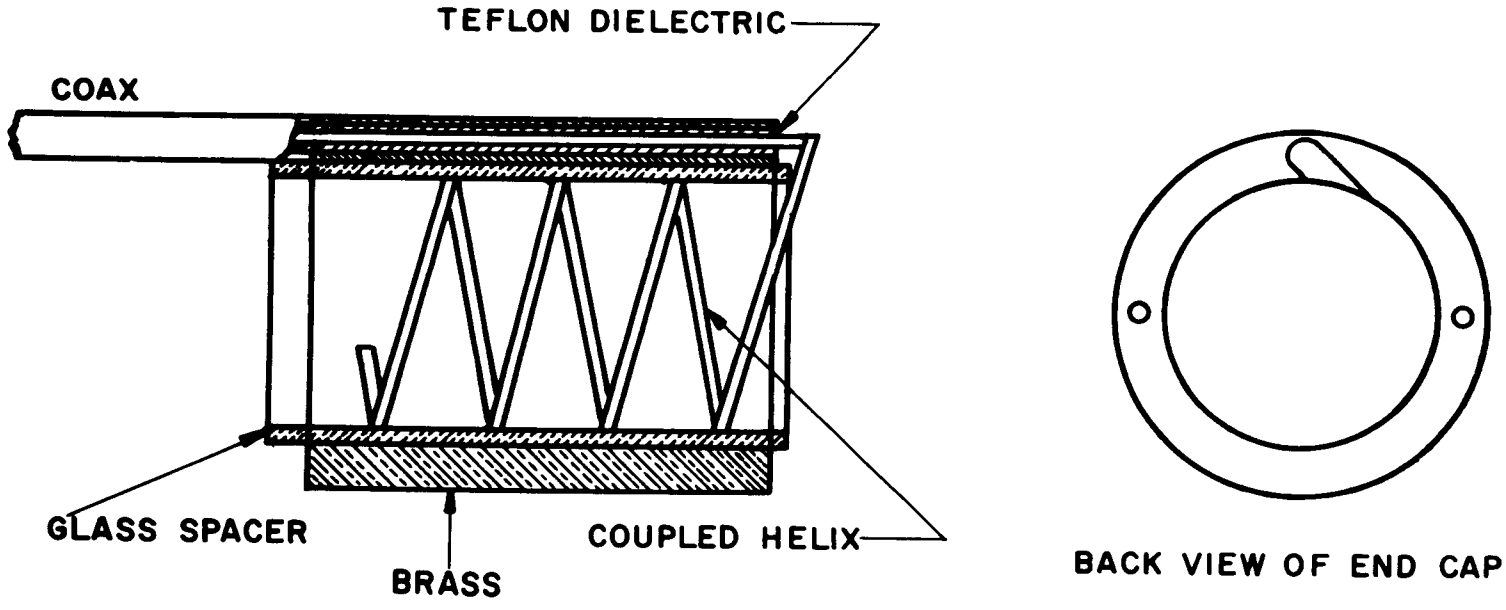


FIG. 9 UHF COUPLER.

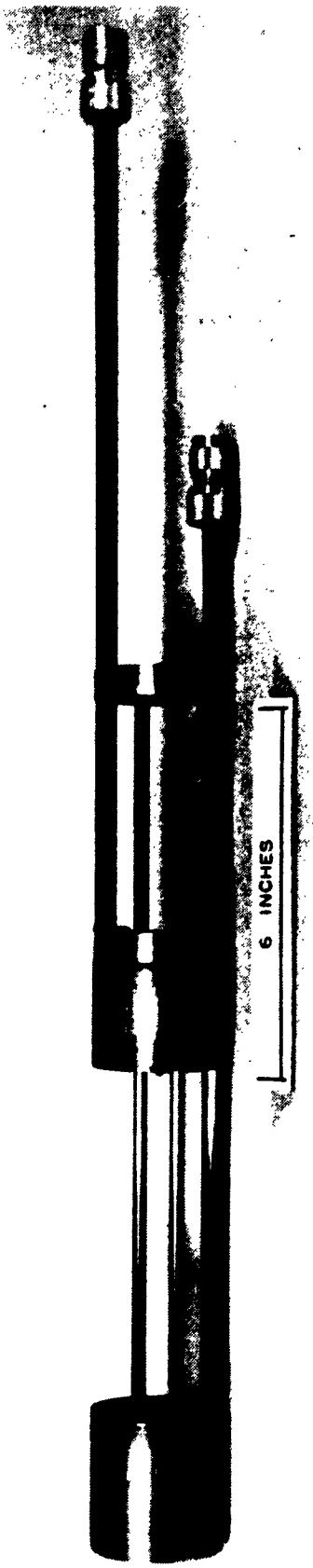


FIG. 10 COUPLER CARRIAGE FOR UHF CRESTATRON.

Table IV

Coupled-Helix Coupler Data

| | |
|---|---|
| T.P.I.: | 2.06 |
| Inside Diameter: | 1.13 inch |
| Wire Diameter: | 0.080 inch |
| Shield Diameter: | 1.50 inch |
| Shield Length: | 2-3/8 inches |
| Turns: | 4 |

Figure 11 shows the VSWR vs. frequency for one coupler with the main helix terminated in a matched load. The insertion loss due to a typical coupler is also shown. Throughout the operating range of the tube (from 300-900 mc) the insertion loss is less than 1 db per coupler and the VSWR is less than 2 to 1 except for a few points. For the modest gain of a Crestatron, however, the reflection coefficients at the couplers can be somewhat higher than for a high-gain tube and still not cause oscillations. For stability it is necessary to meet the relation

$$k_1^2 \, k_2^2 \, G < 1 \quad , \tag{15}$$

where the k's are the input and output reflection coefficients and G is the gain of the tube. If G = 10, as it is approximately in this tube, it may be found that the reflection coefficient must be less than 56 percent for each coupler. This corresponds to a VSWR of 3.5 to 1. From Fig. 11 it may be seen that this criterion is met.

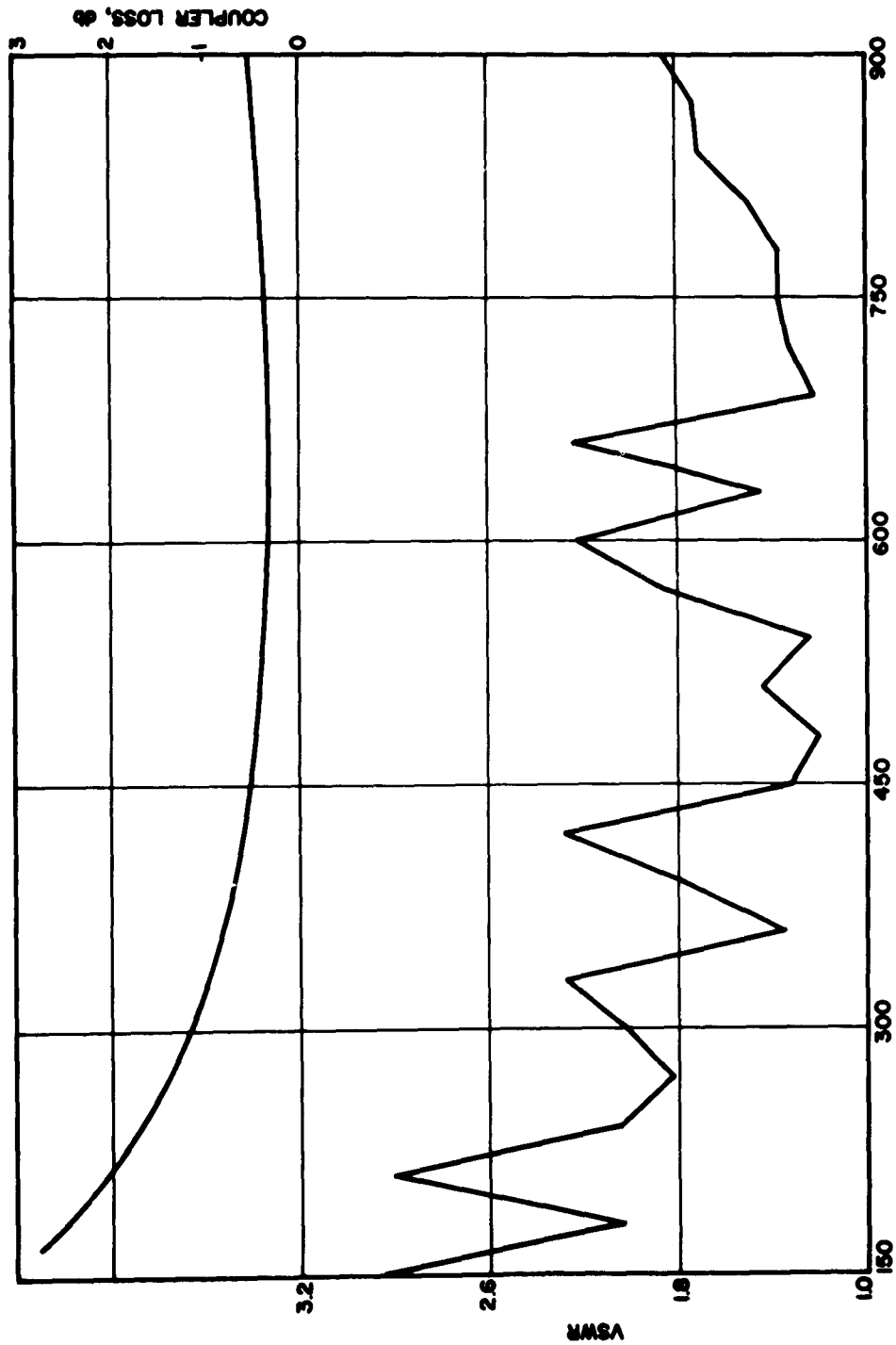


FIG. 11 VSWR AND INSERTION LOSS FOR A TYPICAL COUPLED-HELIX COUPLER USED WITH THE UHF TUBES.

## EXPERIMENTAL RESULTS

The pulser used to power the Crestatron is a line-type modulator. The pulse forming network furnishes a 4 microsecond pulse into a 50-ohm transmission line. In order to achieve a better impedance match into the tube a pulse transformer is employed. The transformer also inverts the polarity of the pulse so that the cathode may be pulsed negative with respect to the helix and collector. Tests were run successfully at both a 250 and 500 pps repetition rate. The beam current transmission and interception may be monitored using average current meters, while the peak cathode voltage is measured across a 100 to 1 vacuum capacitor divider by means of a fast rise-time oscilloscope. A diagram of the experimental test setup is shown in Fig. 12.

In order to completely drive the Crestatron to saturation, a chain of uhf tubes is required. The r-f power source is a General Radio oscillator which puts out several hundred milliwatts. This signal is amplified to several watts in a cw traveling-wave amplifier. The pulsed, 1 kw driver tube is powered by the cw tube. The output of this tube is used to drive the Crestatron. Even though the driver is rated at one kilowatt from 500 to 1000 megacycles, it was found that nearly rated output could be obtained for frequencies as low as 300. A photograph of the test area showing all the associated equipment is shown in Fig. 13.

The first three tubes constructed had an interaction length of 8 inches. Due to the fact that the coupled-helix couplers shorten the effective interaction length, the helix length was increased to 9 inches. Although the tubes were thoroughly baked during processing, it was noted that the vacuum during operation was not very good. Consequently appendage

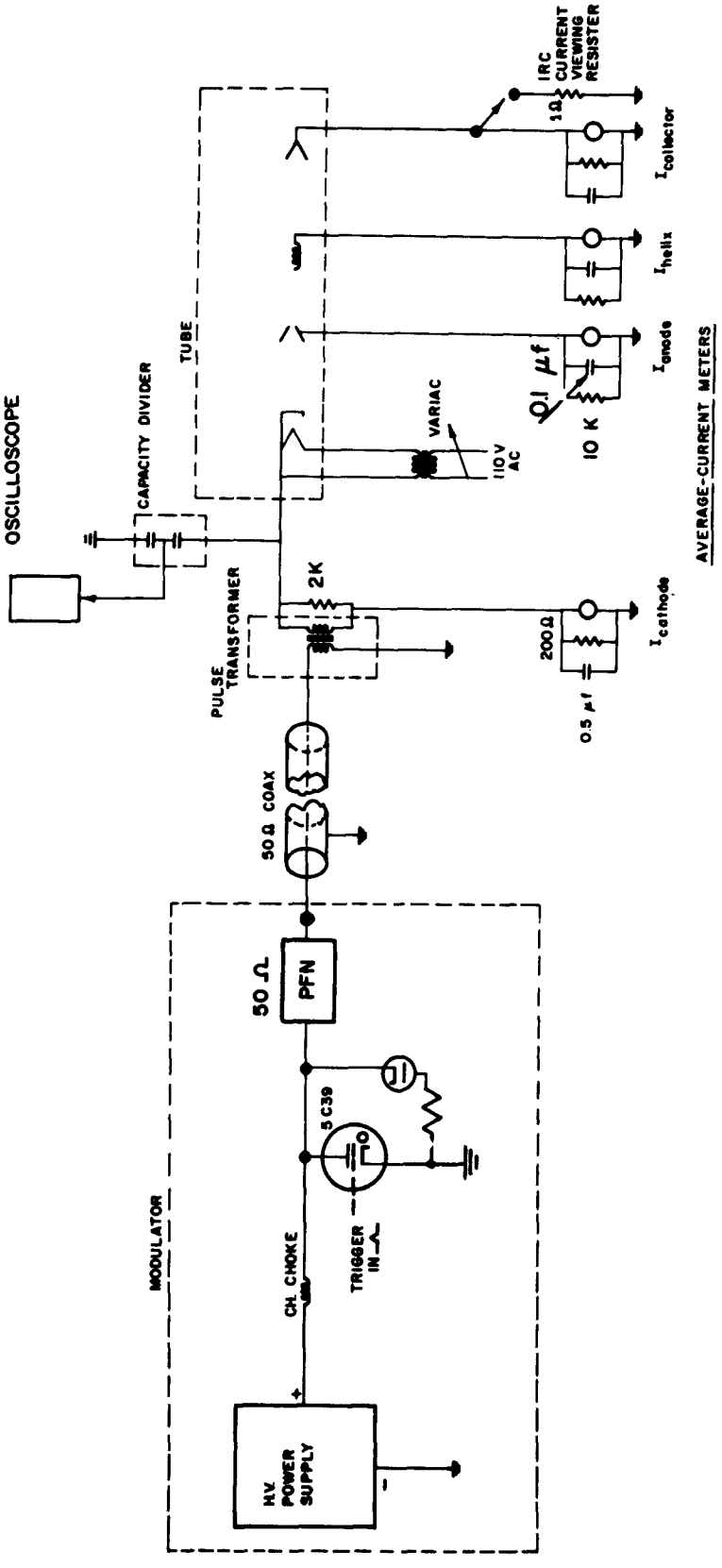


FIG. 12 EXPERIMENTAL TEST SETUP.

FIG. 13 TEST AREA FOR UHF CRESTATRON EXPERIMENTS.

pumps were attached to the later models of the Crestatron. In Fig. 14 may be seen a photograph of one of the completed uhf Crestatrons with a 5 liter/second ion pump attached.

The first tube built, designated the Uhf-1, had a poor beam transmission (≈ 50 percent) and was unstable. Strong forward-wave oscillations were observed near the band edges at 330 and 920 mc. A peak oscillation power of approximately 5 kw was observed at these frequencies. Subsequently the beam transmission became even lower. When this tube was opened, it was found that the three spot welds holding the cathode assembly in place had failed, resulting in a badly tilted cathode.

The Uhf-2 had a much better beam transmission (90 percent) than the first tube. It was possible to take fairly extensive small-signal data before this tube failed because of a crack developing in the envelope near the pump-out stem. Representative small-signal gain curves as a function of operating voltage are shown in Fig. 15. The operating frequency in this case was 650 mc. A maximum gain of 13 db was obtained at a beam voltage of 8.5 kv for the unshielded case, while 12 db was obtained for the shielded helix at a beam voltage of 6.5 kv. The square root of the ratio of these two voltages is approximately equal to the ratio of the two cold phase velocities, as might be expected.

Data taken on the Uhf-3 showed that it had less beam transmission (75 percent) than the second tube and had a much greater tendency to oscillate. In order to reduce these oscillations, which seemed to cover the whole frequency range, it was necessary to add loss. This was done by wrapping teledeltos paper around the envelope, increasing the cold loss from 3 to approximately 7 db. The data obtained in that fashion was found to be quite unmeaningful. Hence the tube was dismantled.

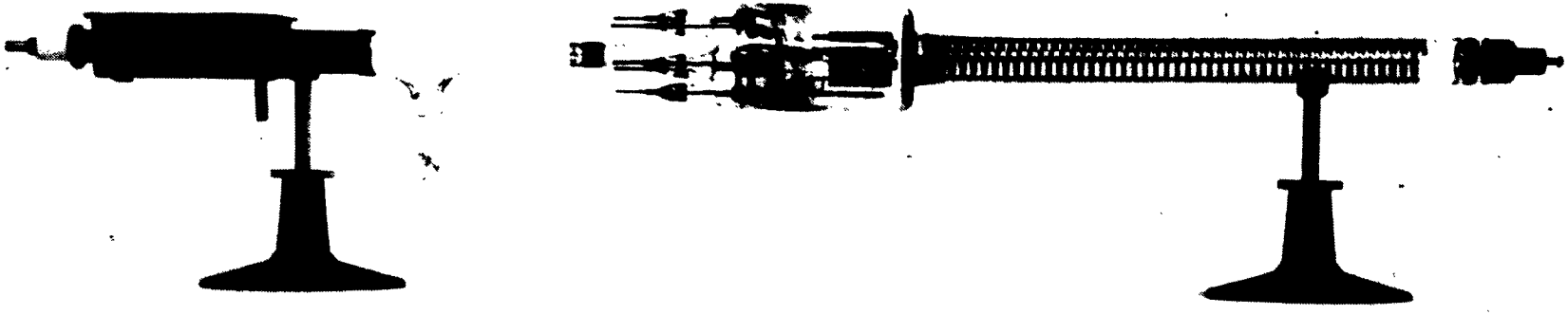

FIG. 14 UHF-5 CRESTATRON.

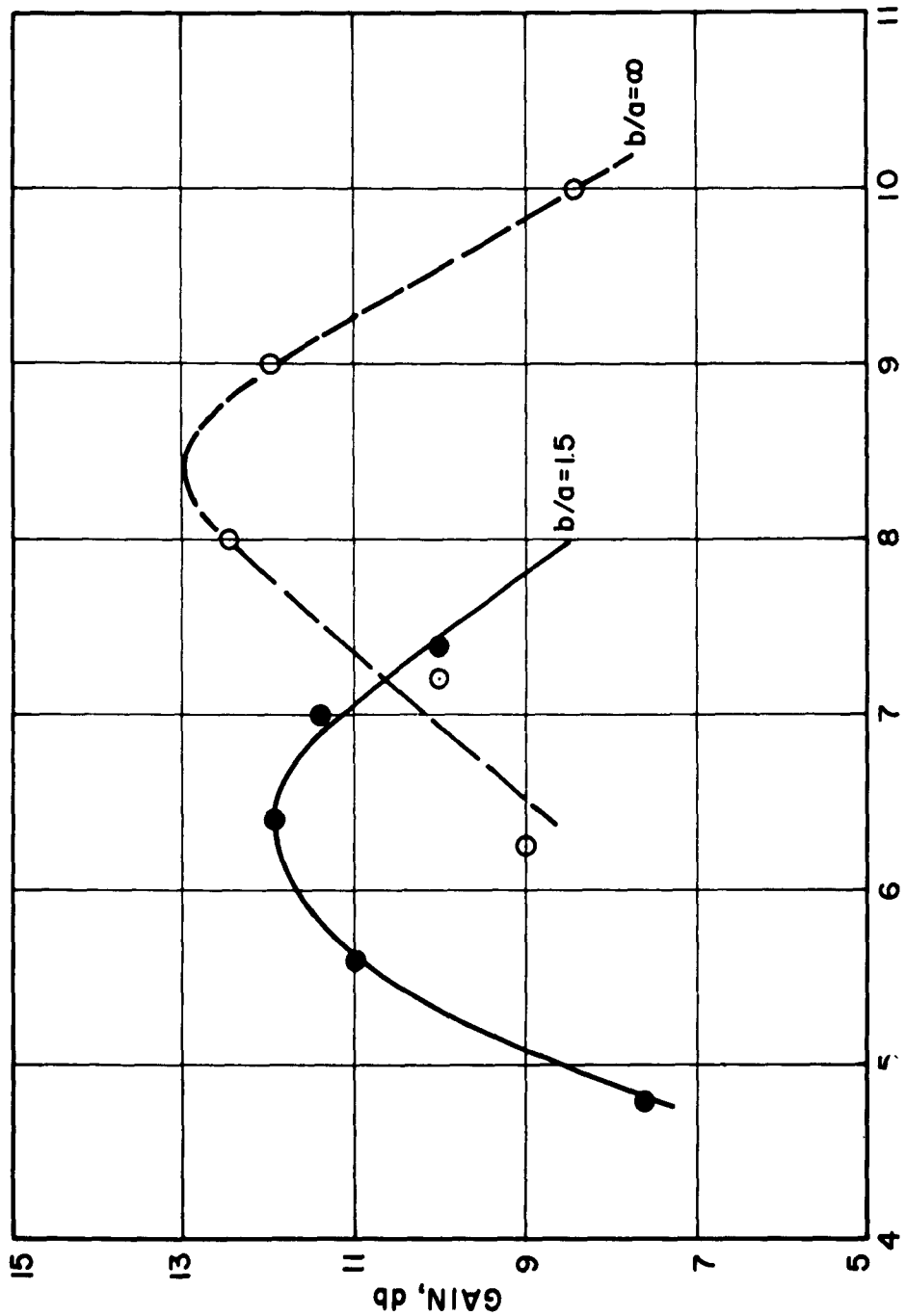


FIG. 15 SMALL-SIGNAL GAIN VS. BEAM VOLTAGE FOR UHF CRESTATRON FOR SHIELDED AND UNSHIELDED HELICES. (FREQUENCY = 650 MC, PULSE LENGTH = 4 μ SEC., PPS. = 250).

The fourth tube, designated the Uhf-4, met all design requirements, even though the beam transmission was not quite as good as that for the Uhf-2. For higher operating voltages in particular, some low-level oscillations were observed across the operating frequency band. These oscillations had a magnitude of only a few tenths of one percent of the beam power and hence did not interfere with gain measurements even in the small-signal region. The cathode emission was at its design value so that 3 amperes could be obtained at a voltage of 6 kv. At 8 kv more than 4 amperes of beam current were observed. This resulted in a peak beam power of greater than 32 kw. With the duty factor set at 0.002, the average power that had to be dissipated in the collector was 64 watts. Cooling was achieved by means of an air blast. The cold loss of the helix is shown in Fig. 16.

Figures 17 and 18 show the small-signal gain curves as a function of frequency. It may be seen that the small-signal gain is quite flat over the entire 3 to 1 frequency range. It was not possible to extend the measurements to lower and higher frequencies due to equipment limitations, found particularly in the driver tube. Over the voltage range of 4 to 8 kv the small-signal gain is seen to vary from approximately 11 to 18 db. For an operating voltage of 7 kv the velocity parameter b can be shown to approach $b_{x_1=0}$ near 750 mc. Thus it may be seen that the transition from the growing-wave to the beating-wave regime is a smooth one.

The small-signal gain observed on the Uhf-4 is higher than is to be expected from a tube with a simple helix as a slow-wave structure. By considering the effect of the coupled-helix couplers in conjunction with the tube helix, it can be shown that an increase in gain is possible due to a growing-wave interaction in the coupler region even though the tube

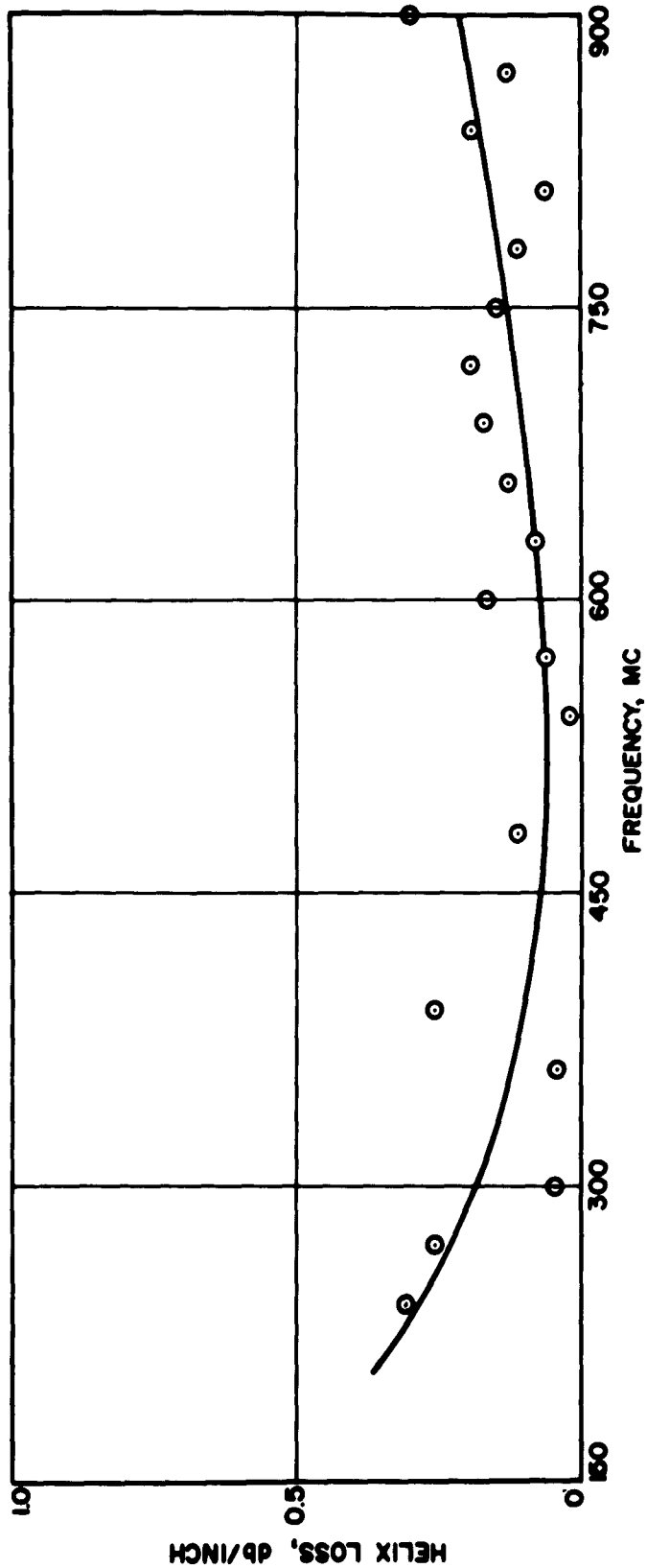


FIG. 16 HELIX LOSS FOR THE UHF CRESTATRON.

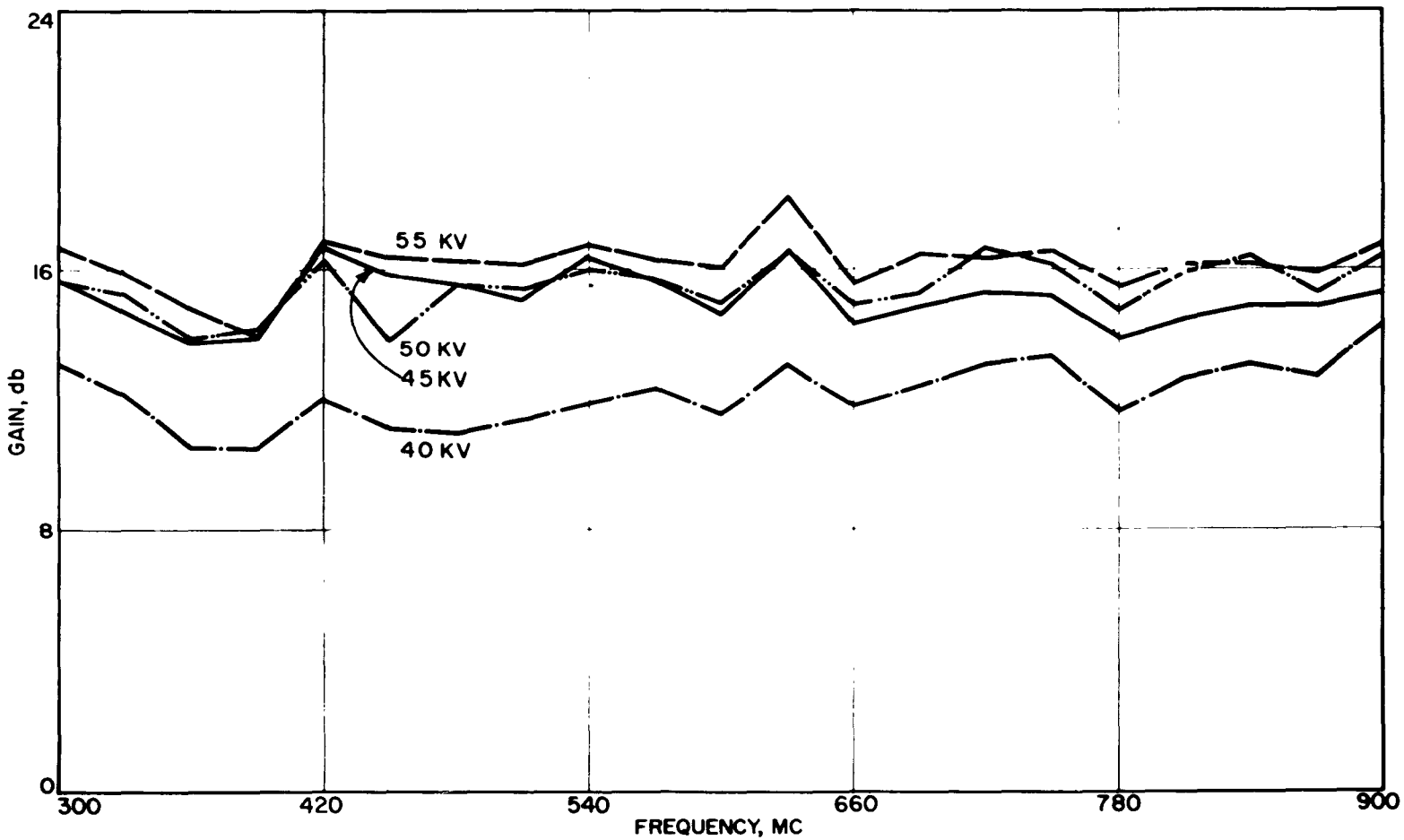


FIG. 17 SMALL-SIGNAL GAIN AS A FUNCTION OF FREQUENCY WITH OPERATING VOLTAGE AS A PARAMETER FOR THE UHF-4.

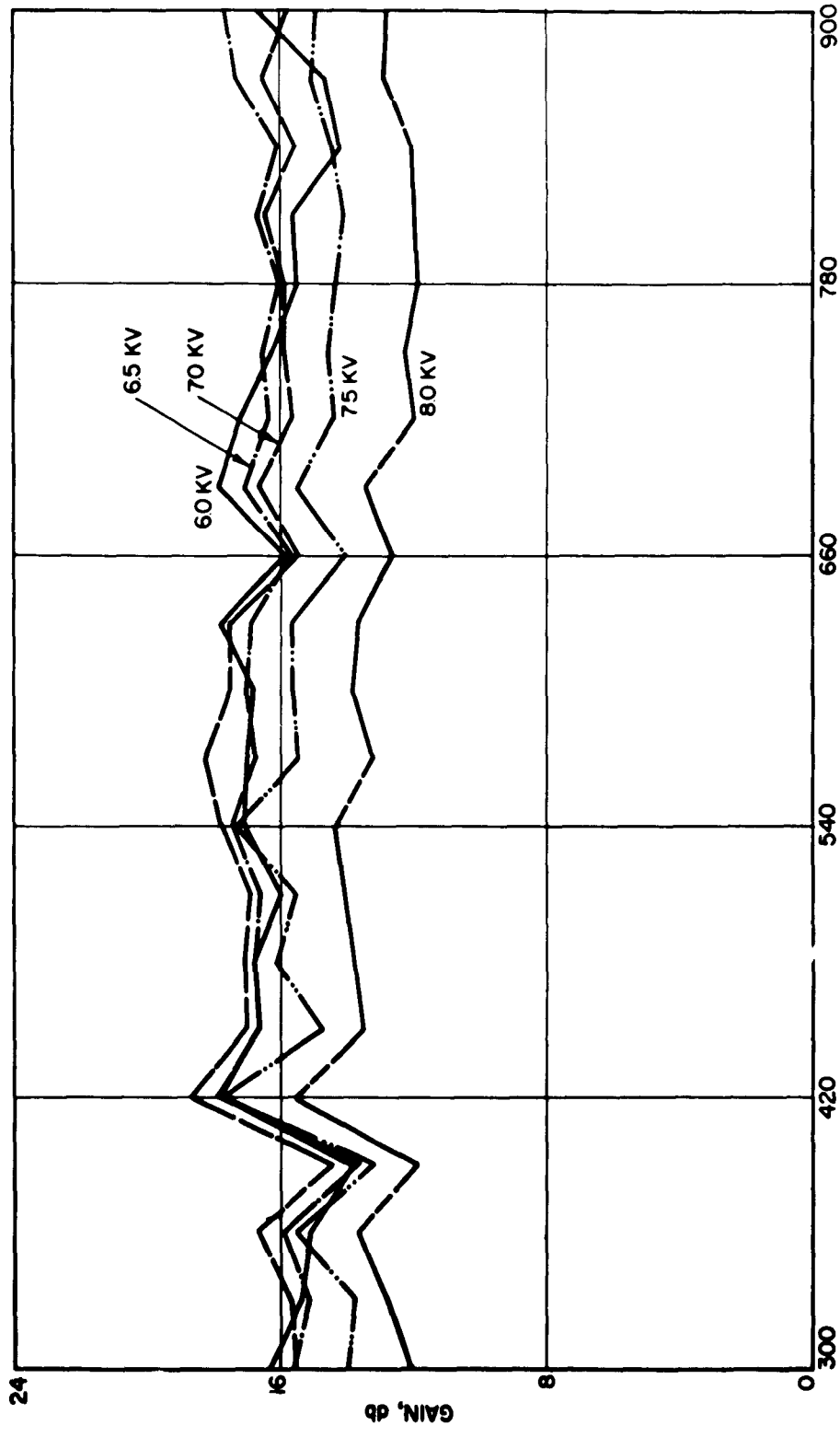


FIG. 18 SMALL-SIGNAL GAIN AS A FUNCTION OF FREQUENCY WITH OPERATING VOLTAGE AS A PARAMETER FOR THE UHF-4.

is operating in the beating-wave regime[8]. Since each coupler is approximately two inches long, a substantial portion of the 9-inch long interaction structure is in reality a system of coupled helices and an increase in gain is possible.

The saturation performance of the Uhf-4 is shown in Figs. 19 through 25. Pertinent operating parameters are listed with each figure. Near saturation the most efficient operation was obtained somewhere in the vicinity of 5 kv. An inspection of the figures also reveals that most efficient operation occurs at the low frequency end of the operating band. A peak power output of 7 kw with 4 or 5 db gain was observed. The maximum conversion efficiency was 27 percent. It should be pointed out that the coupler losses which were in the neighborhood of 0.5 to 1.0 db were corrected for in the data presented. The cold loss of the helix itself, however, is included in the saturation data. Since the input power, $P_i$, to the Crestatron is a substantial portion of the output power, $P_o$, it is necessary to subtract the input power from the output power in a computation of conversion efficiency. The expression used for the determination of the saturation efficiency is

$$\eta_s = \frac{P_o - P_i}{I_o V_o} , \qquad (16)$$

where $I_o$ and $V_o$ are the beam current and voltage, respectively, and where $P_o$ and $P_i$ are adjusted to account for the coupler loss.

Since the cathode had to be operated at 1200° C in order to obtain the beam current densities indicated, the emission dropped off very markedly before data could be obtained for a shielded helix. Consequently it was necessary to open up the tube and reprocess it with a new cathode.

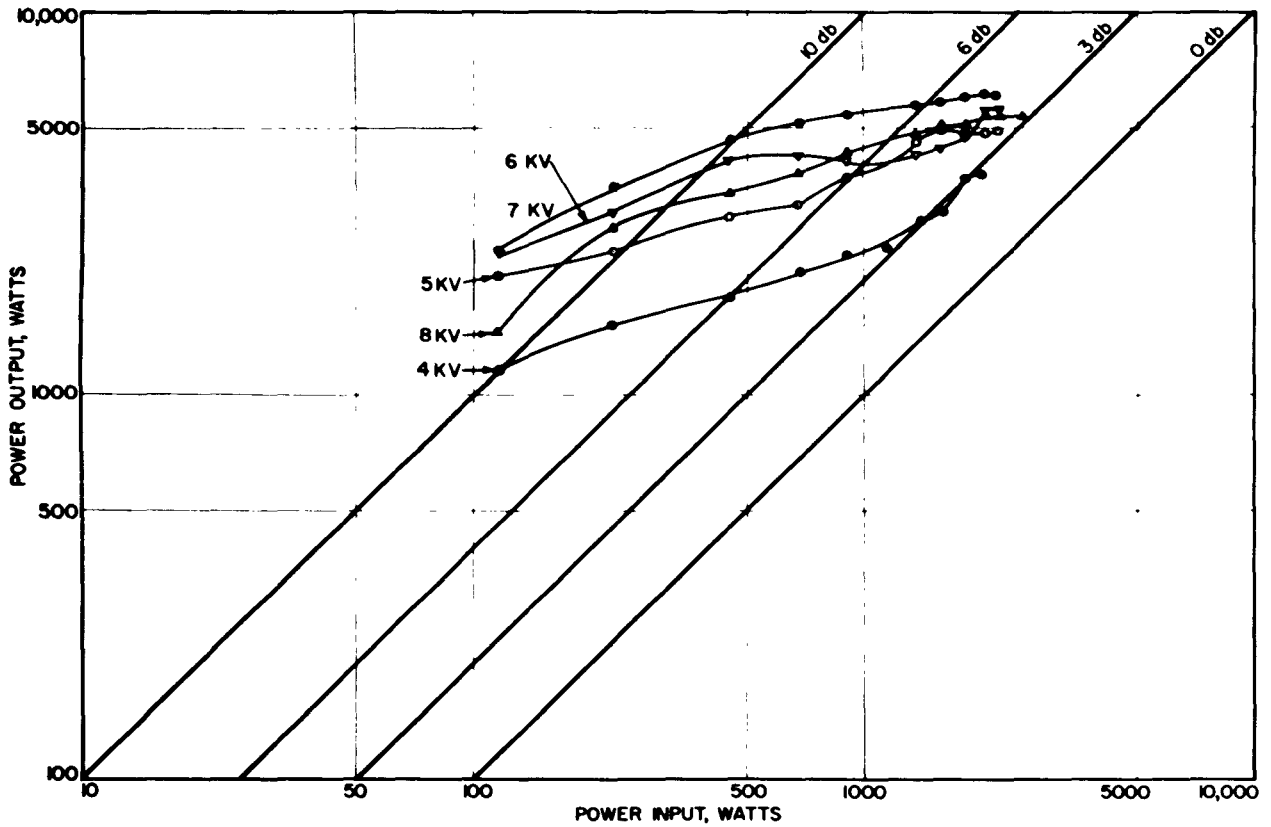


FIG. 19 SATURATION GAIN FOR THE UHF-4 AT 300 MC.

| $V_o$(KV) | $I_o$(amp) | $P_\mu$ | C | QC | b | $\eta_s$(max) |
|---|---|---|---|---|---|---|
| 4.0 | 2.0 | 7.90 | 0.331 | 0.033 | 0.06 | 23.8% |
| 5.0 | 2.5 | 7.08 | 0.331 | 0.036 | 0.38 | 27% |
| 6.0 | 3.0 | 6.45 | 0.331 | 0.039 | 0.71 | 19% |
| 7.0 | 4.0 | 6.83 | 0.346 | 0.043 | 0.95 | 16.2% |
| 8.0 | 4.2 | 5.88 | 0.334 | 0.045 | 1.27 | 10.4% |

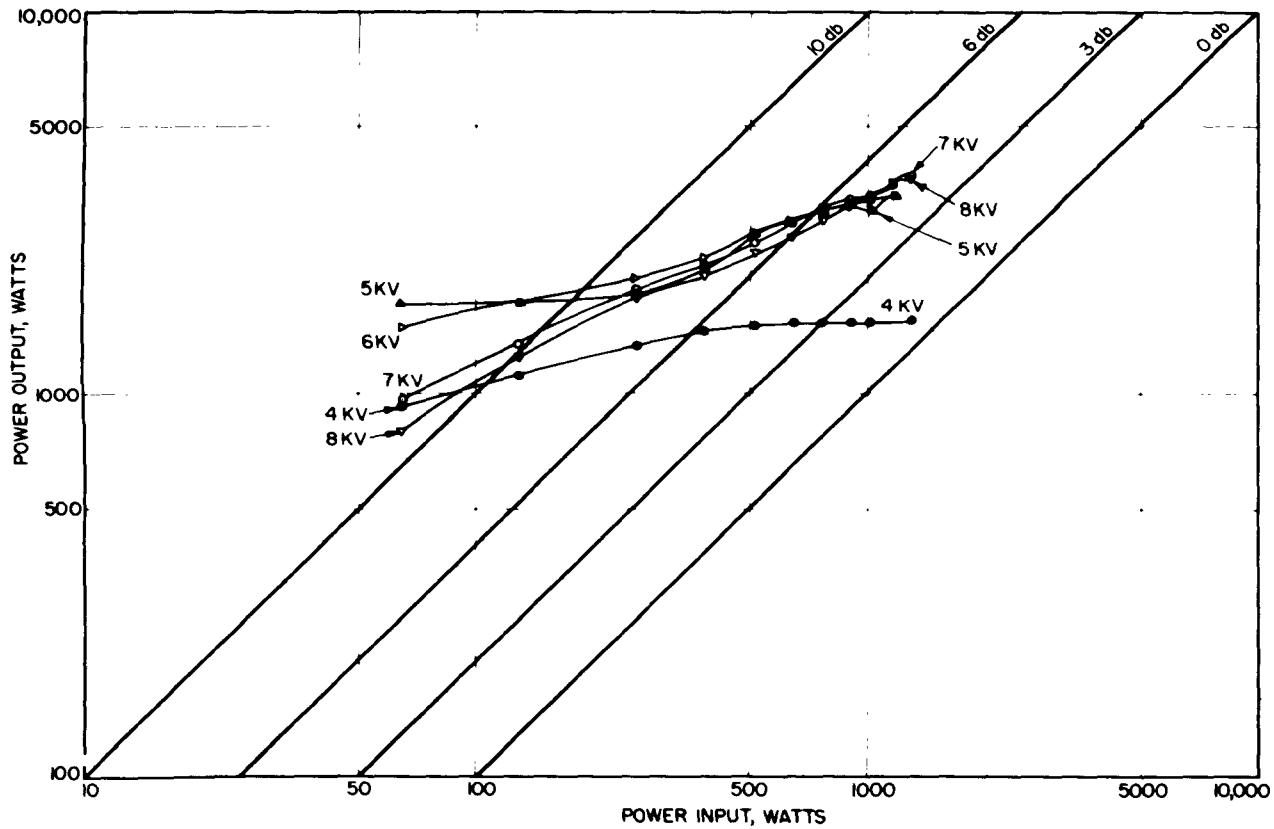


FIG. 20 SATURATION GAIN FOR THE UHF-4 AT 450 MC.

| $V_o$(KV) | $I_o$(amp) | $P_\mu$ | C | QC | b | $\eta_s$(max) |
|---|---|---|---|---|---|---|
| 4.0 | 2.0 | 7.90 | 0.249 | 0.066 | 0.54 | 13.7% |
| 5.0 | 2.5 | 7.08 | 0.249 | 0.072 | 1.08 | 19.2% |
| 6.0 | 3.0 | 6.45 | 0.249 | 0.078 | 1.57 | 12.2% |
| 7.0 | 4.0 | 6.83 | 0.260 | 0.086 | 1.92 | 9.0% |
| 8.0 | 4.2 | 5.88 | 0.253 | 0.089 | 2.38 | 6.8% |

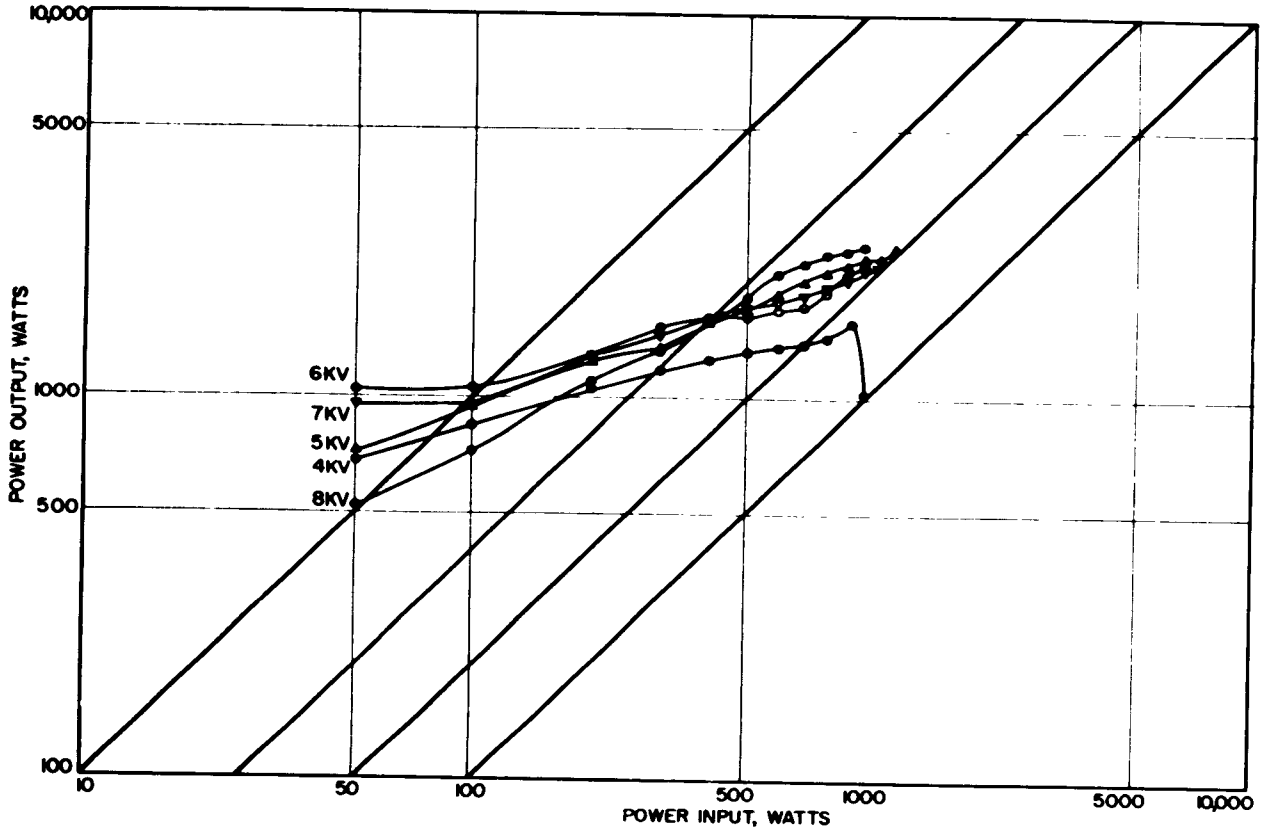


FIG. 21 SATURATION GAIN FOR THE UHF-4 AT 600 MC.

| $V_o$(KV) | $I_o$(amp) | $P_\mu$ | C | QC | b | $\eta_s$(max) |
|---|---|---|---|---|---|---|
| 4.0 | 2.0 | 7.90 | 0.205 | 0.099 | 1.10 | 11.2% |
| 5.0 | 2.5 | 7.08 | 0.205 | 0.108 | 1.80 | 13.4% |
| 6.0 | 3.0 | 6.45 | 0.205 | 0.118 | 2.44 | 6.7% |
| 7.0 | 4.0 | 6.83 | 0.214 | 0.128 | 2.89 | 4.5% |
| 8.0 | 4.2 | 5.88 | 0.208 | 0.134 | 3.51 | 4.1% |

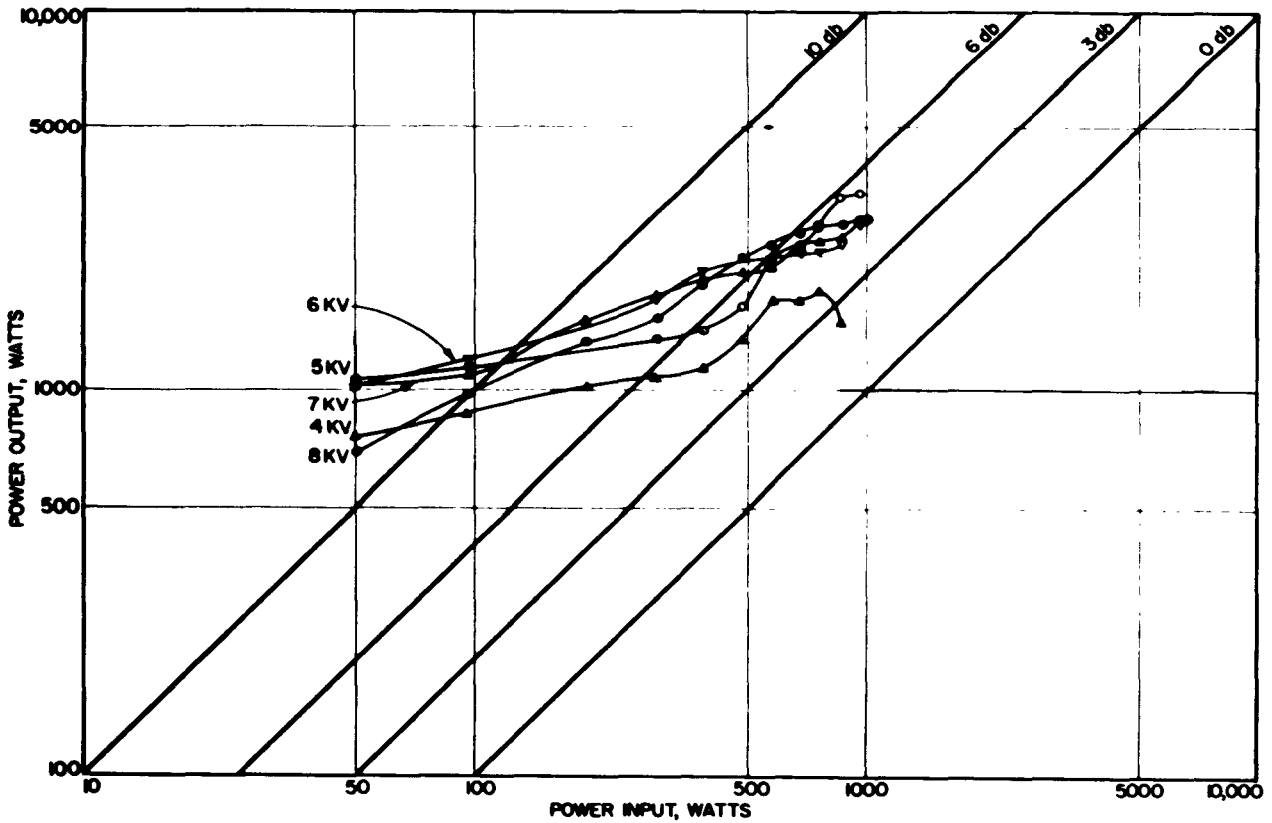


FIG. 22 SATURATION GAIN FOR THE UHF-4 AT 750 MC.

| $V_o$(KV) | $I_o$(amp) | $P_\mu$ | C | QC | b | $\eta_B$(max) |
|---|---|---|---|---|---|---|
| 4.0 | 2.0 | 7.90 | 0.182 | 0.125 | 1.38 | 14.6% |
| 5.0 | 2.5 | 7.08 | 0.182 | 0.137 | 2.18 | 19.4% |
| 6.0 | 3.0 | 6.45 | 0.182 | 0.148 | 2.92 | 9.9% |
| 7.0 | 4.0 | 6.83 | 0.190 | 0.162 | 3.43 | 6.4% |
| 8.0 | 4.2 | 5.88 | 0.185 | 0.169 | 4.17 | 5.6% |

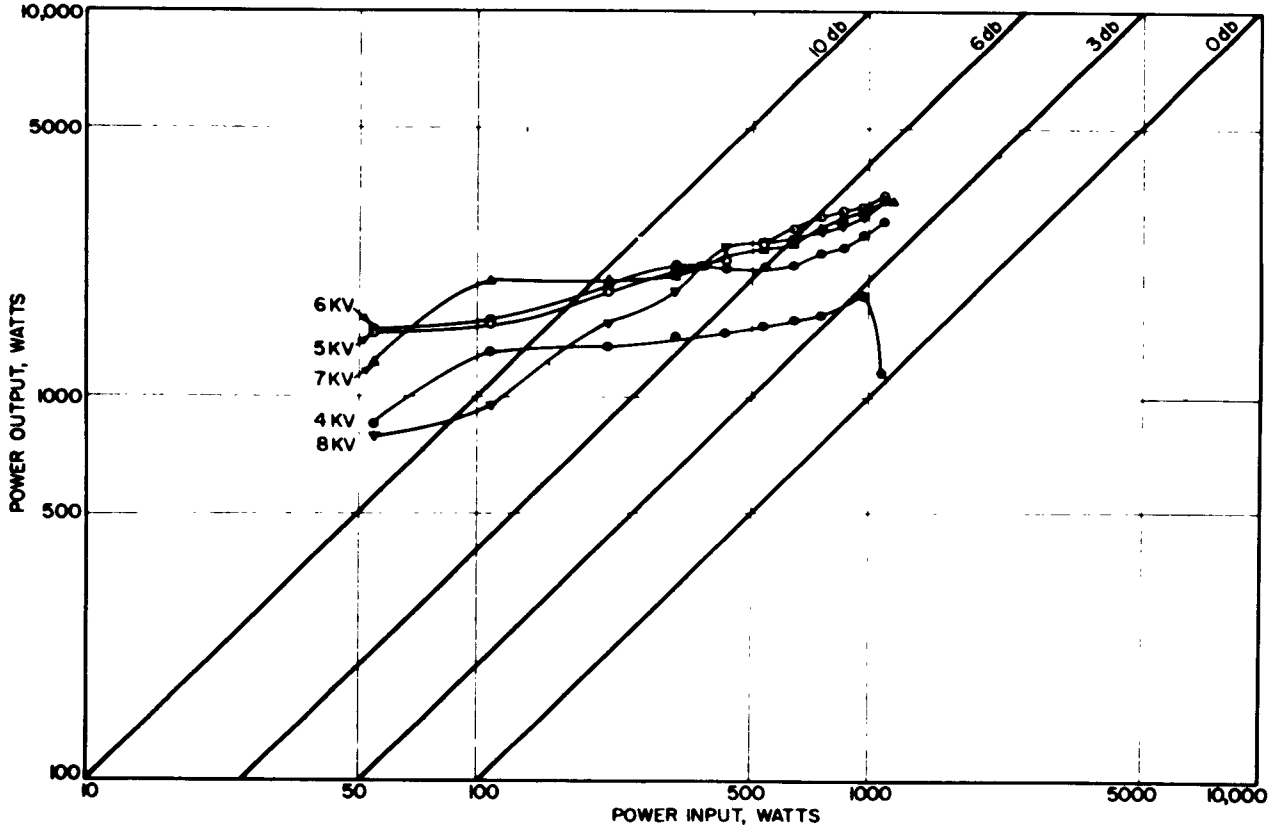


FIG. 23 SATURATION GAIN FOR THE UHF-4 AT 900 MC.

| $V_o$(KV) | $I_o$(amp) | $P_\mu$ | C | QC | b | $\eta_s$(max) |
|---|---|---|---|---|---|---|
| 4.0 | 2.0 | 7.90 | 0.171 | 0.137 | 1.53 | 14.8% |
| 5.0 | 2.5 | 7.08 | 0.171 | 0.151 | 2.40 | 17.6% |
| 6.0 | 3.0 | 6.45 | 0.171 | 0.163 | 3.20 | 10.4% |
| 7.0 | 4.0 | 6.83 | 0.179 | 0.178 | 3.74 | 7.9% |
| 8.0 | 4.2 | 5.88 | 0.174 | 0.186 | 4.50 | 6.6% |

The Uhf-5 had a partially poisoned cathode. In spite of this, fairly complete data was obtained. Gain and saturation measurements were taken for both a shielded as well as an unshielded helix. Due to the low beam current, which was only approximately one third of the design value, the gain of the tube was much lower than for the Uhf-4. Figure 24 shows a comparison between the small-signal gain of the shielded helix and the unshielded one. As is to be expected, the tube with a shield ($b/a = 1.5$) has a lower gain due to its lower interaction impedance and lower gain parameter, C. On the other hand the gain curve as a function of frequency may be seen to be flatter due to the reduced dispersion of the r-f structure. Since C is low for this tube, the saturation efficiency may be expected to also be quite low. Figure 25 confirms this.

Since the tubes investigated have a relatively wide bandwidth, the harmonic generation would be of considerable interest to a systems designer. If the input signal is 300 mc, for example, both the second and third harmonics are within the operating band of the tube and hence there would be some output at 600 as well as 900 mc. From klystron theory the expression for the harmonic content for a bunched beam is well known and may be written as

$$\frac{|i_m|}{I_o} = 2J_m(mX) \quad , \tag{17}$$

where $i_m$ and $I_o$ are the mth harmonic current and the d-c current, respectively, while $J_m$ is the mth order Bessel function, and X is the bunching parameter. For the first few harmonics and a degree of bunching commonly encountered in traveling-wave tubes the harmonic content of the bunched beam is seen to increase with the degree of bunching. Thus a tube operating near saturation may be expected to put out a considerable amount of

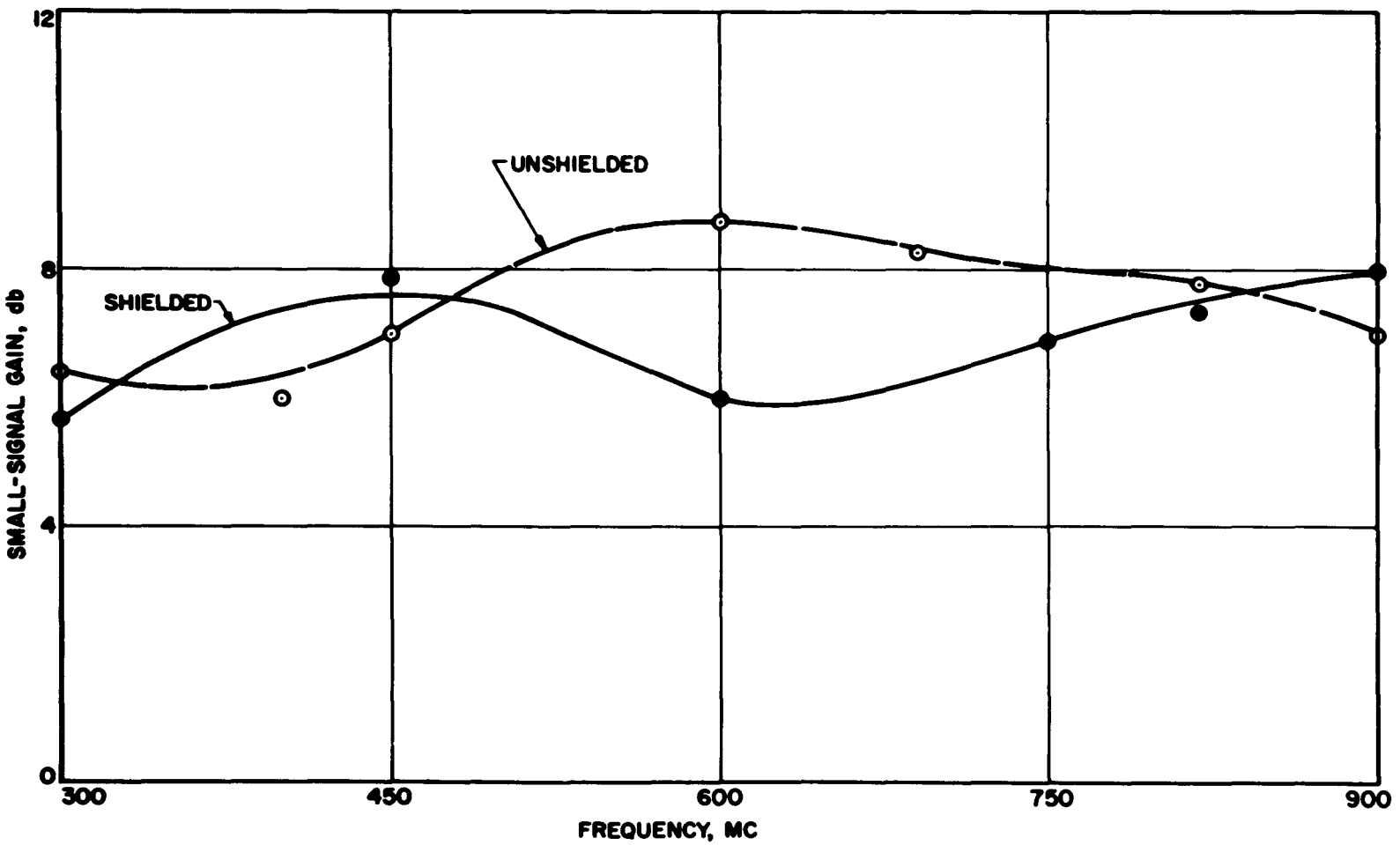


FIG. 24 SMALL-SIGNAL GAIN AS A FUNCTION OF FREQUENCY FOR THE UHF-5 CRESTATRON AT 7.0 KV.

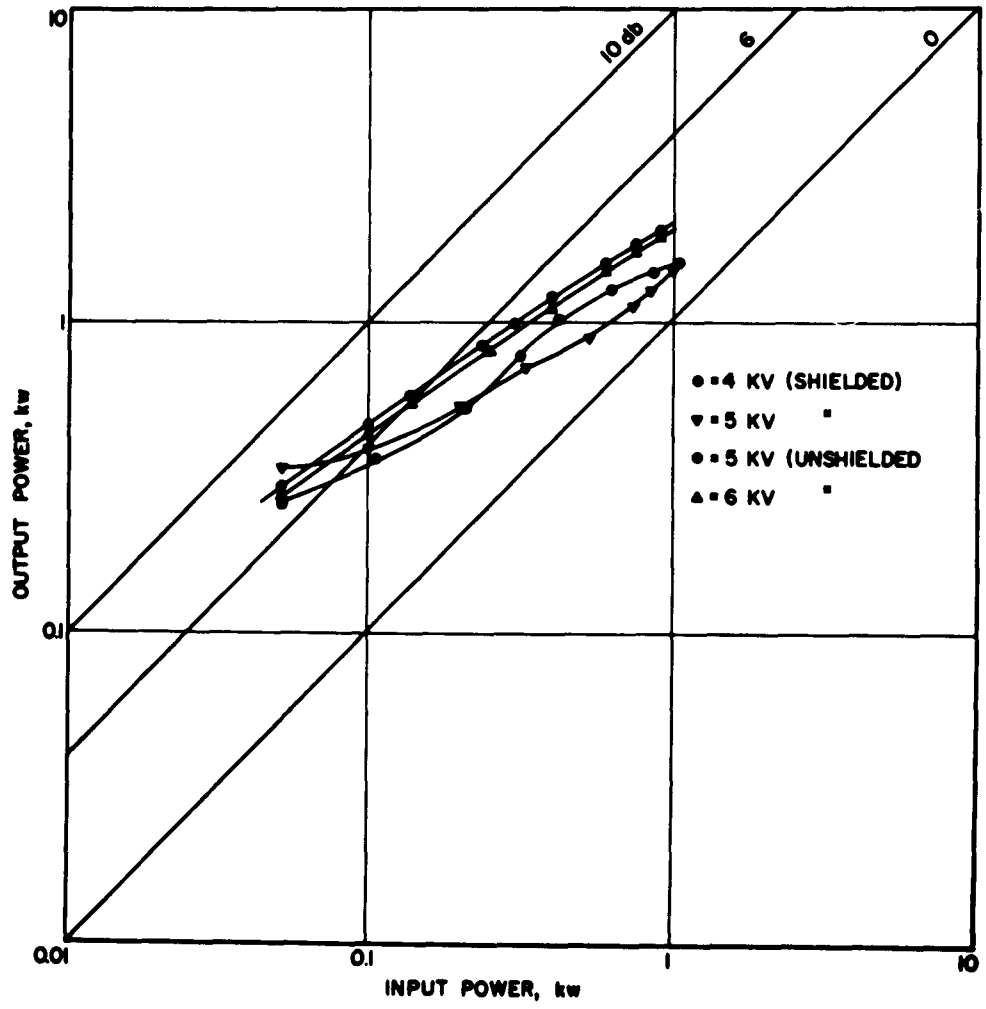


FIG. 25 SATURATION CHARACTERISTICS FOR THE UHF-5 CRESTATRON FOR A SHIELDED AND UNSHIELDED HELIX AT 450 MC.

| $V_o$ (Volts) | $I_o$ (Amps) | C | QC | b | $\eta_{max.}$ (Percent) | b/a |
|---|---|---|---|---|---|---|
| 4.0 | 1.15 | 0.160 | 0.101 | 1.85 | 14.4 | 1.5 |
| 5.0 | 1.68 | 0.168 | 0.116 | 3.50 | 6.6 | 1.5 |
| 5.0 | 1.28 | 0.230 | 0.046 | 1.18 | 15.9 | ∞ |
| 6.0 | 1.38 | 0.222 | 0.049 | 1.76 | 12.0 | ∞ |

power at the harmonic frequencies. Measurements were taken on the Uhf-5 to substantiate this. The results are shown in Figs. 26 through 28. With an input power sufficient to drive the tube far into saturation, it may be seen that the second harmonic output at certain frequencies may only be approximately 3 db down from the fundamental output power, while under the same conditions the third harmonic output power may be 12 to 14 db down. Under small-signal conditions the harmonic content is seen to be quite small.

Assuming a value of $|i_1|/I_o = 1.0$, which is reasonable for a traveling-wave device near saturation, it is possible to compute the harmonic output from Eq. 17. The ratio of harmonic power to fundamental power may be related to the current ratios by $i^2K_o$, where $K_o$ is the interaction impedance at the frequency under consideration. In Fig. 29 the theoretical and experimental curves are shown. The reason for the discrepancy between the two curves is that space-charge effects do not allow the bunching in the tube to be ideal. A rectangular bunch, as is assumed in the theory, is difficult to obtain in practice.

## CONCLUSIONS

A high-power, pulsed Crestatron was constructed to operate in the uhf range. The theory of operation of this device has been presented and a design procedure outlined. The experimental results obtained from the tubes built indicate that wideband Crestatron operation is possible at uhf frequencies using a short r-f structure, 2-4 wavelengths long. A reasonably flat small-signal gain of approximately 15 db has been obtained over a 3 to 1 bandwidth. Peak power outputs in excess of 5 kw and

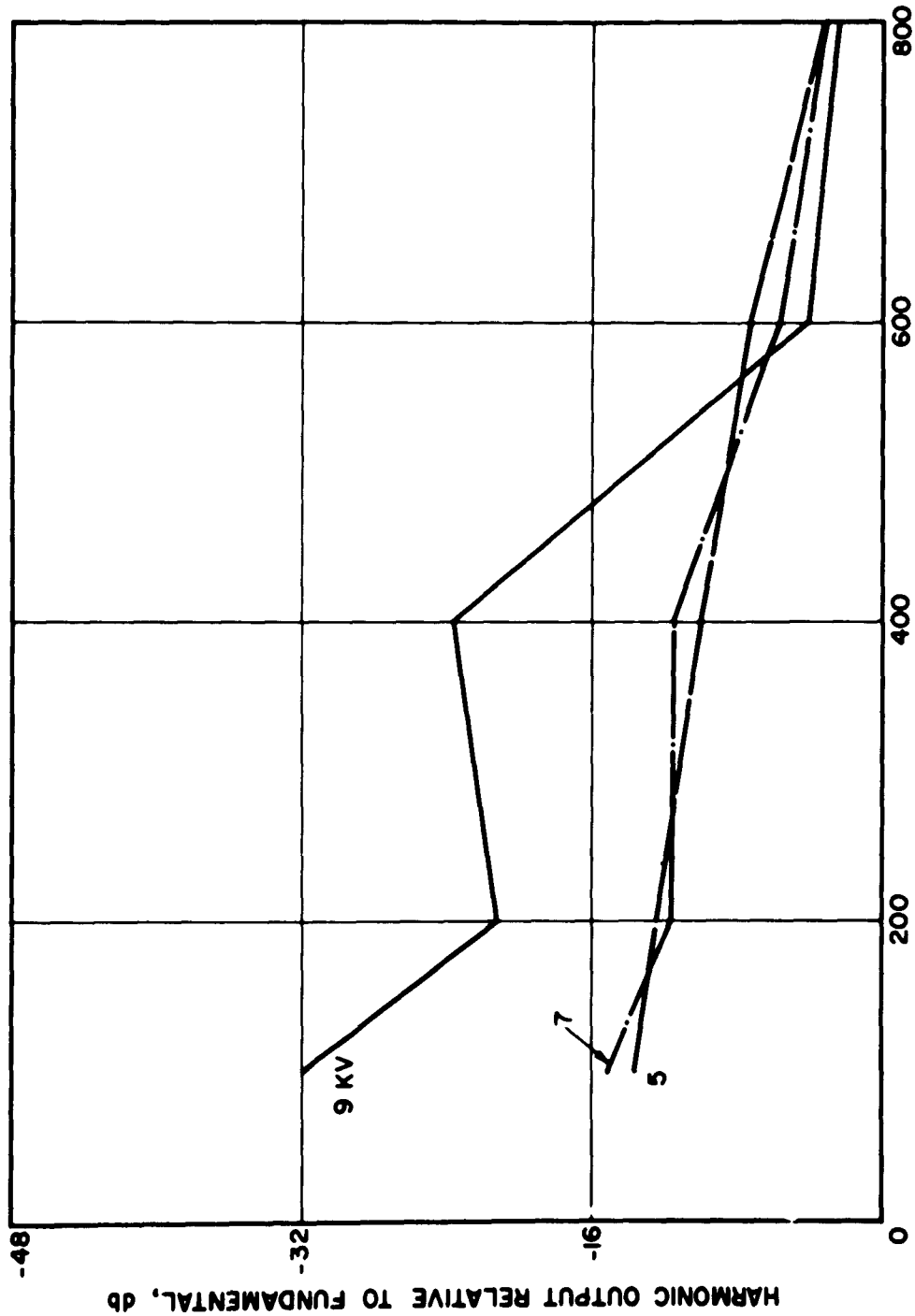


FIG. 26 SECOND HARMONIC CONTENT OF THE UHF-5 OUTPUT POWER WITH 300 MC INPUT.

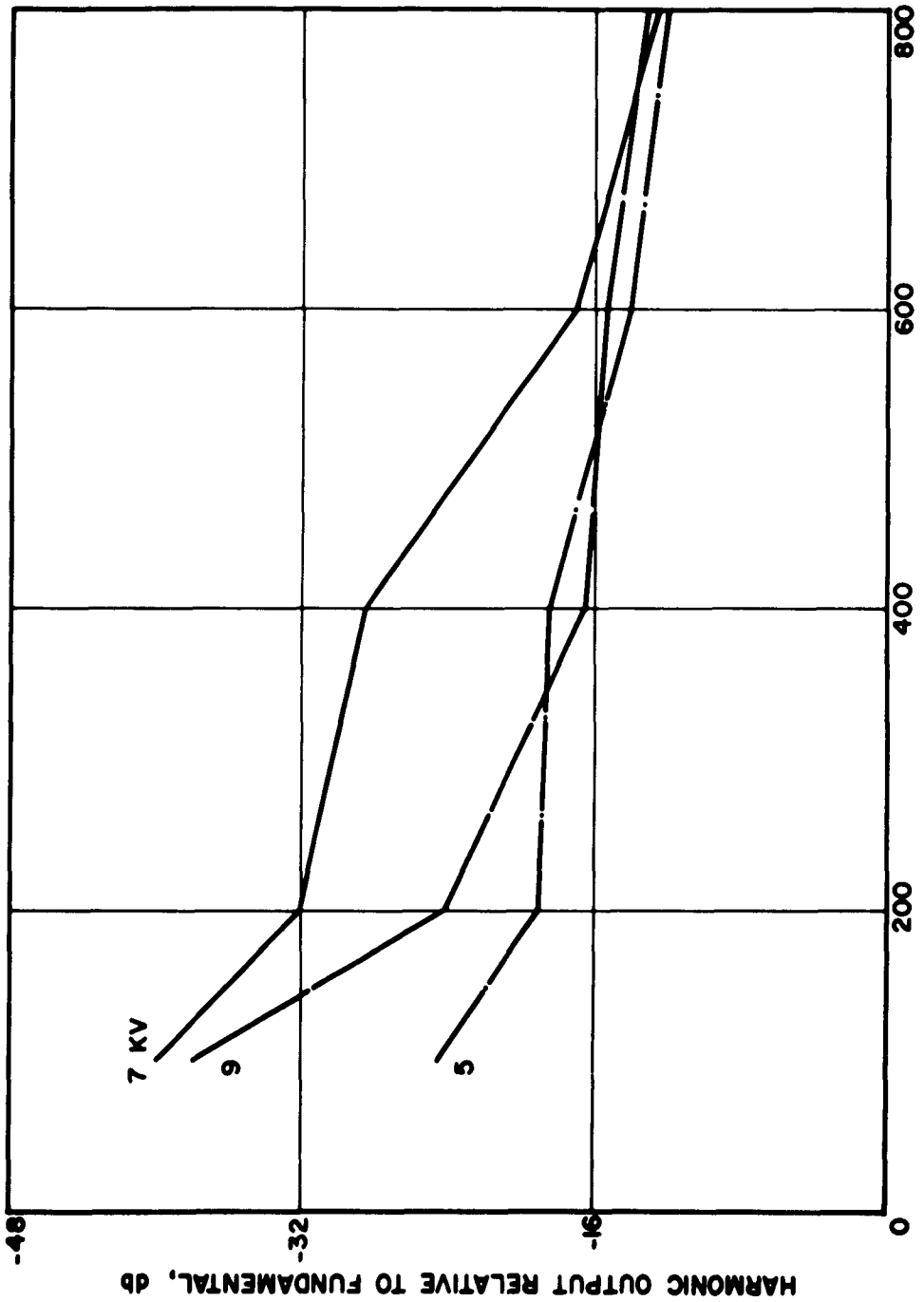


FIG. 27 THIRD HARMONIC CONTENT OF THE UHF-5 OUTPUT POWER WITH 300 MC INPUT.

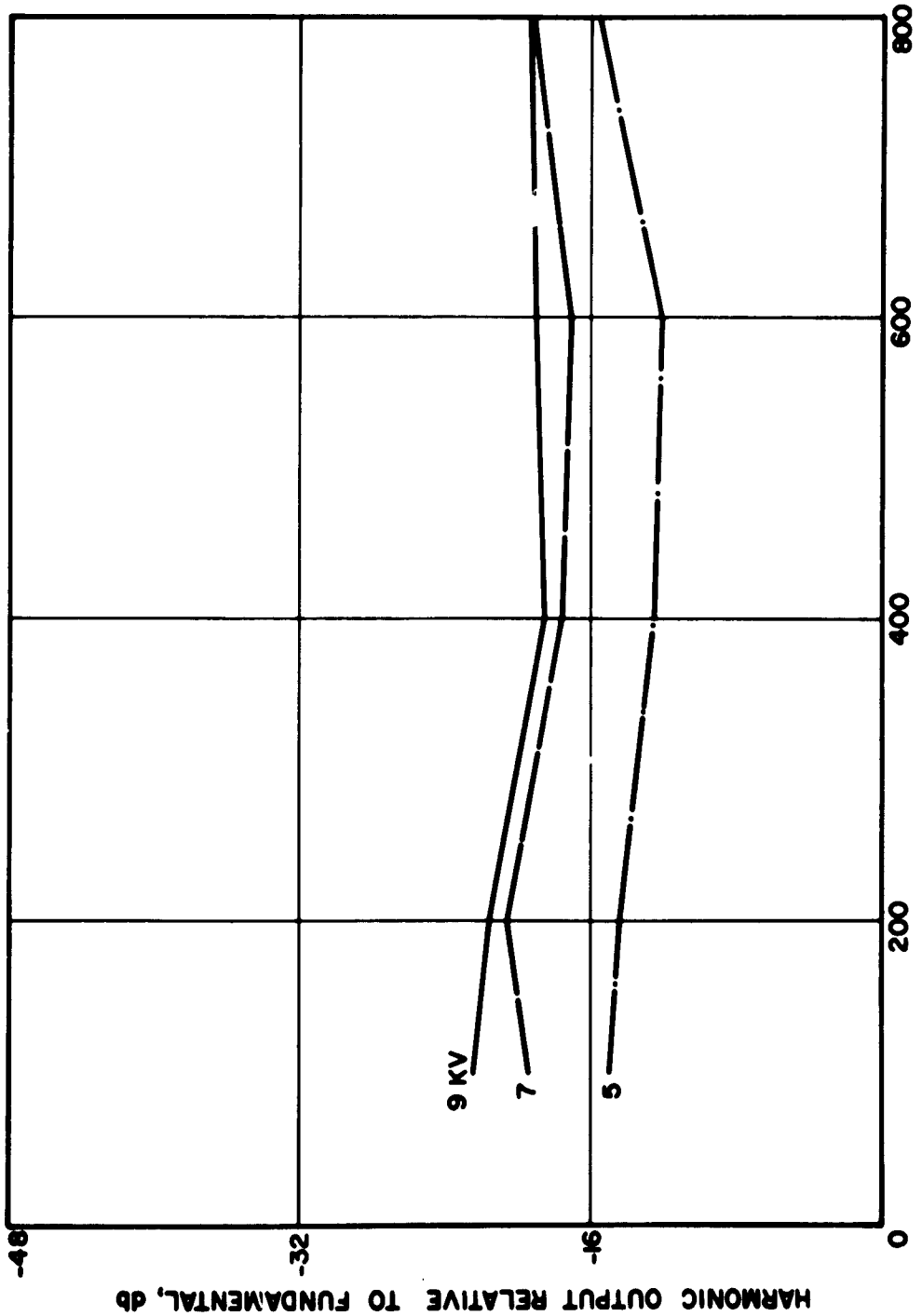


FIG. 28 SECOND HARMONIC CONTENT OF THE UHF-5 OUTPUT POWER WITH 450 MC INPUT.

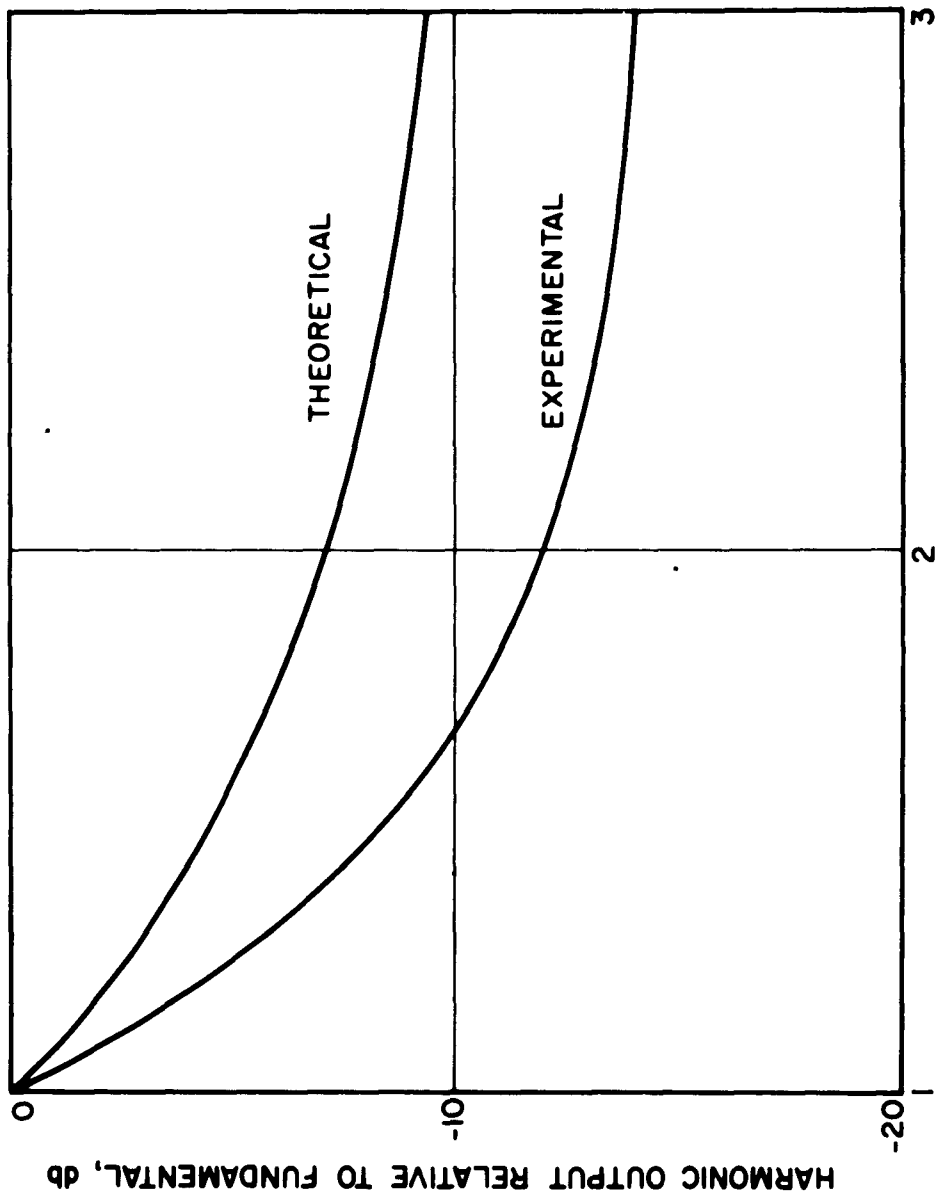


FIG. 29 HARMONIC OUTPUT OF THE UHF-5 CRESTATRON NEAR SATURATION WITH A FUNDAMENTAL INPUT POWER OF 300 MC.

saturation efficiencies as high as 27 percent were observed. The low-level oscillations are believed to be due to imperfect coupler matches.

Data showing the harmonic content of the Crestatrons is presented. The other factors of interest to systems designers such as cross-modulation, intermodulation and phase characteristics are not available from these tubes due to a lack of adequate test facilities and due to the low-level oscillations described above.

## LIST OF REFERENCES


1. Rowe, J. E., "Theory of the Crestatron: A Forward-Wave Amplifier", Proc. IRE, vol. 47, No. 4, pp. 536-545; April, 1959.
2. Branch, G., Mihran, T., "Plasma Frequency Reduction Factors in Electron Beams", Trans. PGED-IRE, vol. ED-2, No. 2, pp. 3-11; April, 1955.
3. Jones, E. M. T., "A Negative Dispersion Helix Structure", Electron Research Laboratory, Stanford University, Tech. Rpt. No. 27, p. 3; August 7, 1950.
4. Ayers, W. R., "High Power Applications of the Connected Ring Structure in Traveling Tubes", Microwave Laboratory, Stanford University, Rpt. No. 554, p. 126; December, 1958.
5. Rowe, J. E., op. cit., Reference 1.
6. Lagerstrom, R. P., "Interaction-Impedance Measurements by Perturbation of Traveling Waves", Electronics Laboratory, Stanford University, Tech. Rpt. No. 7; February 11, 1957.
7. Mathers, G., Kino, G., "Some Properties of a Sheath Helix with a Center Conductor or External Shield", Electronics Research Laboratory, Stanford University, Tech. Rpt. No. 65; June 17, 1953.
8. Yeh, C., "Helix Couplers for Linear-Beam Devices", Trans. PGED-IRE, vol. ED-9, No. 1, pp. 69-75; January, 1962.

## CATALOGUE FILE CARD

Rome Air Development Center, Griffiss AF Base, NY Rpt No. RADC-TDR-62-446, THE DESIGN AND CONSTRUCTION OF A HIGH-POWER UHF CRESTATRON, Progress Rpt No. 1, Aug 62, 51p incl illus, tables.
Unclassified Report

The design, construction and experimental tests of a pulsed, high-power uhf Crestatron are described. The design procedures outlined in this report are useful for the construction of Crestatrons in general. The data presented shows the operating characteristics of the Crestatron under small-signal as well as large-signal conditions. In addition some experiments on the harmonic output of the Crestatron are described.

1. Principles of Crestatron Operation
2. General Design Considerations
3. Construction and Cold Tests
4. Experimental Results

I. AFSC Project 5573, Task 557303
II. Cont AF 30(602)-2834
III. Elec. Phys. Lab. The University of Michigan, Ann Arbor, Michigan
IV. Konrad, G.T.
V. Secondary Rpt No. TR-52
VI. In ASTIA collection

Rome Air Development Center, Griffiss AF Base, NY Rpt No. RADC-TDR-62-446, THE DESIGN AND CONSTRUCTION OF A HIGH-POWER UHF CRESTATRON, Progress Rpt No. 1, Aug 62, 51p incl illus, tables.
Unclassified Report

The design, construction and experimental tests of a pulsed, high-power uhf Crestatron are described. The design procedures outlined in this report are useful for the construction of Crestatrons in general. The data presented shows the operating characteristics of the Crestatron under small-signal as well as large-signal conditions. In addition some experiments on the harmonic output of the Crestatron are described

1. Principles of Crestatron Operation
2. General Design Considerations
3. Construction and Cold Tests
4. Experimental Results

I. AFSC Project 5573, Task 557303
II. Cont AF 30(602)-2834
III. Elec. Phys. Lab. The University of Michigan, Ann Arbor, Michigan
IV. Konrad, G.T.
V. Secondary Rpt No. TR-52
VI. In ASTIA collection

Rome Air Development Center, Griffiss AF Base, NY Rpt No. RADC-TDR-62-446, THE DESIGN AND CONSTRUCTION OF A HIGH POWER UHF CRESTATRON, Progress Rpt No. 1, Aug 62, 51p incl illus, tables.
Unclassified Report

The design, construction and experimental tests of a pulsed, high-power uhf Crestatron are described. The design procedures outlined in this report are useful for the construction of Crestatrons in general. The data presented shows the operating characteristics of the Crestatron under small-signal as well as large-signal conditions. In addition some experiments on the harmonic output of the Crestatron are described.

1. Principles of Crestatron Operation
2. General Design Considerations
3. Construction and Cold Tests
4. Experimental Results

I. AFSC Project 5573, Task 557303
II. Cont AF 30(602)-2834
III. Elec. Phys. Lab. The University of Michigan, Ann Arbor, Michigan
IV. Konrad, G.T.
V. Secondary Rpt No. TR-52
VI. In ASTIA collection

Rome Air Development Center, Griffiss AF Base, NY Rpt No. RADC-TDR-62-446, THE DESIGN AND CONSTRUCTION OF A HIGH-POWER UHF CRESTATRON, Progress Rpt No. 1, Aug 62, 51p incl illus, tables.
Unclassified Report

The design, construction and experimental tests of a pulsed, high-power uhf Crestatron are described. The design procedures outlined in this report are useful for the construction of Crestatrons in general. The data presented shows the operating characteristics of the Crestatron under small-signal as well as large-signal conditions. In addition some experiments of the harmonic output of the Crestatron are described.

1. Principles of Crestatron Operation
2. General Design Considerations
3. Construction and Cold Tests
4. Experimental Results

I. AFSC Project 5573, Task 557303
II. Cont AF 30(602)-2834
III. Elec. Phys. Lab. The University of Michigan, Ann Arbor, Michigan
IV. Konrad, G.T.
V. Secondary Rpt No. TR-52
VI. In ASTIA collection